The stratigraphic and structural record of the Cretaceous Jianghan Basin, central China: Implications for initial rifting processes and geodynamics

Lulu Wu [a], Lianfu Mei [a]*, Yunsheng Liu [b], Douglas A. Paton [c], Jin Luo [b], Lu Yu [a], Deliang Wang [a], Caizheng Min [d], Minghua Li [b], Libin Guo [b], Hui Wen [b]

[a] Key Laboratory of Tectonics and Petroleum Resources, Ministry of Education, China University of Geosciences, Wuhan 430074, China

[b] Research Institute of Exploration and Development of Jianghan Oilfield, SINOPEC, Wuhan 430000, China

[c] Basin Structure Group, School of Earth and Environment, University of Leeds, Leeds, LS2 9JT, UK

[d] Research Institute, China National Offshore Oil Corporation (CNOOC), Beijing 10027, China

*Corresponding author: Lianfu Mei, E-mail: lfmei@cug.edu.cn

Abstract

The stratigraphic and structural characteristics of the initial phase of continental rift basins have been widely studied. However, the initial rifting geodynamic processes in many rift basins remain poorly understood because the relevant structures and stratigraphic successions tend to be deeply buried in result of continued rift evolution. Using an extensive database of geological (stratigraphic and structural) and geophysical data we investigate when and how rift initiation occurred in the

Jianghan Basin. The correlation of the Early Cretaceous strata across the basin reveals that they were deposited within a series of localized depressions distributed on the basin margin while the Late Cretaceous tectonic stage was characterized by widespread rifting with a maximum stratal thickness of ~4500 m. The major faults controlling this Late Cretaceous sediment distribution are radially striking, suggesting a distributed, transtensional stress system or multi-directional extension during the Late Cretaceous. It is a common feature that pre-rift basement strata of the major faults in the hanging wall are older than that in the footwall and become progressively older approaching the fault plane, indicating a reactivation of pre-existing unroofed fault-related folds. Together with the regional geodynamic context for the South China Block, we divide the initial rifting processes into two distinct stages. During the Early Cretaceous, the lithosphere beneath the Jianghan Basin got rapidly thinned under the influence of the large-scale roll-back and dehydration of the subducted Pacific slab. Meanwhile, the upwelling asthenosphere and intruded dykes/magma heated and weakened the lithosphere, leading to thermal doming of the most region of the Jianghan Basin. However, on the basin margin, which was relatively unaffected by the thermal doming event, a set of localized depression sequences were deposited. Due to the Early Cretaceous lithospheric thinning, the lithosphere was thin enough to rift during the Late Cretaceous. Under the diapirism of the continuously upwelling asthenospheric mantle, the pre-existing thrusts with radial strikes simultaneously underwent extensional reactivation, forming a series of normal faults with multiple orientations. By providing the detailed stratigraphic and structural evidence for active rifting model, this study provides new insights into the processes of early rift initiation.

Keywords: Stratigraphic record; Structural record; Lithospheric thinning; Reactivation; Rift

initiation; Jianghan Basin

1. Introduction

The Wilson cycle is accepted as a key element of plate tectonics whereby compressional margins are extended and subsequently compressed (Wilson, 1966; Buiter and Torsvik, 2014). Most evidence comes from field observations and as a consequence of the superposition of a number of tectonic events, it is often not recognized within sub-surface data. Continental rift basins offer a unique opportunity to investigate how a Wilson cycle initiated after one terminated. However, this question involving the timing, processes and geodynamics of rift initiation is not well resolved in many rift basins (e.g., northern North Sea, Bell et al., 2014; Pearl River Mouth Basin, Gong, 2014; Orphan Basin, Gouiza et al., 2015; Orange Basin, South Africa, Mohammed et al., 2017; Mid-Norwegian margin, Peron-Pinvidic and Osmundsen, 2016; Songliao Basin, Wang et al., 2016). This is primarily because the stratigraphic and structural records associated with rift initiation 1) are not complete (Nottvedt et al., 1995), 2) become deeply buried during continued rifting evolution and 3) are difficult to observe in field, seismic and borehole data (Bell et al., 2014). Some studies provide detailed analysis on the evolution prior to rifting, however, these studies have no detailed analysis on the rifting characteristics during the initial phase (Avni et al., 2012; Miller and Lizarralde, 2013). In contrast, although some studies have investigated the early development of rift basins (Gawthorpe and Leeder, 2000; Gawthorpe et al., 2003; Cowie et al., 2005; Paton, 2006; Rohais et al., 2007; Rajchl et al., 2009; Ford et al., 2013; Henstra et al., 2015, 2016; Nixon et al., 2016), they are mainly focused on fault linkage and interaction, and tectono-sedimentary evolution, with limited discussion on the timing and dynamics of rift initiation. The typical dynamic models for the initiation of continental rifting have been classified into active and passive rifting (Sengor and Burke, 1978). Compared to passive rifting, active rifting is characterized by pre-rift thermal doming, magmatism and deposition (Nottvedt et al., 1995; Corti et al., 2003; Ziegler and Cloetingh, 2004; Avni et al., 2012). Although, in most cases, geochemical or geophysical data provide an answer (Omar and Steckler, 1995; Frey et al., 2007; Natali et al., 2011; Putirka and Platt, 2012; Rooney et al., 2013; Yu et al., 2015), further stratigraphic and structural evidence for supporting either of them is still urgently needed. Hence, the fundamental question concerning the processes, temporal and spatial variation of tectono-sedimentary evolution and geodynamics of the birth of many rift basins, remains unanswered.

The Jianghan Basin (Figs. 1A and 2) in central China provides an excellent opportunity to investigate the initial development of continental rift basins, since (a) its post-rift sequences are relatively thin (< 1100 m, Fig. 3) and remain a terrestrial setting, leading to a relatively shallow burial depth; (b) both the structures and stratigraphic successions associated with rift initiation and pre-rift basement are well preserved and outcrops on the margin of the basin allow facies to be investigated (Fig. 2; HBGMR, 1990; Shi et al., 2013; Li et al., 2014b). As the initial phase of rifting, the Cretaceous evolution of the Jianghan Basin has been widely discussed (Liu et al., 2003, 2005, 2015; Li et al., 2006, 2012b, 2014b; Wang et al., 2006, 2013a; Mei et al., 2008; Zhang et al., 2012; Liu and Zhang, 2013; Shi et al., 2013). Some authors proposed that during the Early Cretaceous the Qinling-Dabie Orogenic Belt continued to extrude southwestward and deform the pre-rift basement with local sedimentation and the Jianghan Basin began to extend during the Late Cretaceous (Liu et al., 2003; Liu and Zhang, 2013; Shi et al., 2013; Wang et al., 2013a). In contrast, other authors proposed limited rifting during the Early Cretaceous resulting in localized deposition on the basin margin, and then accelerated rifting during the Late Cretaceous (Li et al., 2006). However, these conclusions are commonly inconsistent with broader observations. On the one hand, during the Early Cretaceous, the Qinling-Dabie Orogenic Belt and Jiangnan Orogen were characterized by widespread magma intrusion (Fig. 2) and extensional deformation, implying an extensional tectonic setting (e. g., Chen et al., 2009; Li et al., 2014a; Ji et al., 2017b, 2018), so their extrusion may be terminated after the Jurassic. Moreover, the Lower Cretaceous intrusive and volcanic rocks are widespread in the Daye region and close to the south of the Qinling-Dabie Orogenic Belt (Fig. 2), indicating significant extension (Li et al., 2009, 2014b; Xie et al., 2011). On the other hand, the Early Cretaceous stratigraphic successions were conformably overlain by that of Upper Cretaceous deposits (HBGMR, 1990; Wang et al., 2013a), implying that the tectonic settings of these two periods are similar. This conformable sequence is incompatible with a tectonic switch from compression to extension during the Cretaceous. However, the enhanced rifting model that requires sedimentation purely on the basin edge at rift initiation stage is inconsistent with classical rift development model (Prosser, 1993; Cowie, 1998; Gupta et al., 1998; Gawthorpe and Leeder, 2000; Cowie et al., 2005), which predicts that multiple distributed and isolated faults develop during the initial phase of rifting. Perhaps most importantly, existing published studies on the Cretaceous stratigraphic and structural characteristics of the Jianghan Basin are not regional in context, and lack a comprehensive understanding between the evolution of the Jianghan Basin and South China Block.

To address these issues, we use field outcrops, drilling and 2D and 3D seismic data in combination to constrain the timing, distribution and characteristics of extensional deformation of the Cretaceous Jianghan Basin. This paper aims to (1) investigate the stratigraphic and structural features of the Cretaceous Jianghan Basin, (2) document how pre-existing structures underwent extensional reactivation and control basin architecture, and (3) unravel the initial rifting processes and geodynamics. The main significance of this paper is to illustrate active rifting processes by answering when and how rifting initiated in the Jianghan Basin.

2. Geological setting

The tectonic configuration of much of eastern China is controlled by the North-South Gravity Lineament (NSGL; Ma, 1989) that has been attributed to the western extent of the stagnant Pacific slab in the mantle transition zone (Fig. 1; Huang and Zhao, 2006). The position of the lineament is not only associated with a surficial sharp elevation contrast in eastern China (Fig. 1A) but also steep gradients in crustal and lithosphere thickness and heat flow (Guo et al., 2014). The formation of the NSGL mainly contributed to the destruction (characterized by widespread extensional basin generation and voluminous magma intrusion/eruption, Zhu et al., 2015) of the North China Craton and South China Block (Li et al., 2015; Zhu et al., 2015). During the destruction processes, the long-term dehydration (from Triassic to Cretaceous) of the subducted Pacific slab (Niu, 2005; Windley et al., 2010; Li et al., 2012a) has been crucial in weakening and thinning the lithospheric mantle, resulting in the significant differences in lithospheric thickness (> 150 km to west of the NSGL and ca. 80 km to east of the NSGL; Li et al., 2012a, 2015; Zhu et al., 2015). The Jianghan Basin is immediately adjacent to the NSGL and is surrounded in its entirety with compressional systems (Fig. 2), including the Qinling-Dabie Orogenic Belt in the north and northeast, the Edong fold-thrust belt in the east, the Jiangnan Orogen on its southern border and the Huangling Massif and Xiang'exi fold and thrust belt to the west. The petroliferous Jianghan Basin, which represents the Cretaceous-Cenozoic rift basin, covers an area of approximately 28,000 km^2.

The tectonic evolution of the Jianghan Basin records the superimposition of three discrete stages of tectonic evolution (Fig. 3), namely, passive margin, foreland basin and rift basin phases. From the Late Neoproterozoic to the Early Triassic, the Jianghan Basin was situated on the northern continental passive margin of the South China Block with deposition being dominated by thick carbonate platform deposits, marine shale and shallow-marine sandstone (HBGMR, 1990). The collision between the South China Block and South Qingling Belt occurred in Mid-Late Triassic times along the Mianlue suture zone (Dong et al., 2011), which resulted in the transition from a passive margin to a compressional margin that resulted in the initiation of a series of foreland basins on the edge of the South China Block (Dong et al., 2011; Shen et al., 2012a; Liu et al., 2015). The Middle Triassic-Jurassic foreland deposits are mainly characterized by terrestrially deposited conglomerates, sandstones, siltstones and mudstones. Although regional compression continued during the Late Jurassic, the presence and obstruction of the Huangling Massif (Ji et al., 2014; Liu et al., 2015) resulted in a change in regional strain accommodation, which caused near synchronous extrusion of the Qinling-Dabie Orogenic Belt southwest-ward and the Jiangnan Orogen nearly northward (Liu et al., 2015). A consequence of this was the widespread thrusting, folding and denudation of the Sinian to Middle Jurassic strata, which represents the pre-rift basement/sequences for this study. These thrust faults and folds were gradually and extensionally reactivated during the Cretaceous (Mei et al., 2008) and unconformably covered by the Cretaceous deposits. In a similar manner to the widespread rifting observed across the South China Block, the Jianghan Basin underwent a phase of extension associated with the rollback of the subducted Pacific slab (Yang et al., 2012; Li et al., 2014b, 2015). The Jianghan Basin experienced three-phase rifting through the Cretaceous and Paleogene prior to aborting in the Neogene. The basin fill during the Late Cretaceous (syn-rift 1) was dominated by conglomerate, sandstone, mudstone and some basaltic eruptions, while that of the Paleogene rifting (syn-rift 2-3) was mainly sandstone, mudstone, salt and voluminous basaltic eruptions (Fig. 3; Wang et al., 2006). The deposits deposited during the final, post-rift stage, are very thin and have a maximum thickness of 1050 m, dominated by sandstone and conglomerates.

3. Data and Methods

The seismic database used in this study includes > 8000 km of 2-D seismic reflection lines and ca. 5000 km^2 3-D seismic reflection surveys (Fig. 4). The line spacing of 2-D seismic data varies from 1 to 7 km and these 2-D surveys image to depths of 5 to 6 s two way travel time (TWTT). The 3-D seismic reflection surveys image to depths of between 5 and 6 s TWTT and have an inline and crossline spacing of 12.5 m or 25 m. Of particular importance for this study is the generally high quality of the imaging within the pre-rift sequences. Of the 1600 exploration wells in the basin, more than 120 (Fig. 4) penetrated the Late Cretaceous strata and/or pre-rift basement and were used for seismic-well ties and depth-conversion using synthetic seismograms. Based on the seismic and borehole data, pre-rift basement strata and structures are well constrained (Fig. A1). Thickness maps were created using two depth-converted seismic horizons. In addition to mapping of reflections, fault cutoffs were mapped using reflection terminations and hanging wall and footwall cutoff locations were used to define fault polygons and therefore the position, strike and length of major faults. Time-depth conversion are used when calculating stratal thickness and fault dip angles.

Geological field mapping was undertaken in the north Jianghan Basin (Fig. 4) to acquire structural and stratigraphic data of both syn-rift and pre-rift stratigraphy which supplemented existing field data in previous studies (HBGMR, 1990; Tian et al., 2010; Qiao et al., 2012; Shi et al., 2013).

4. Characteristics of Early and Late Cretaceous extension

4.1. Cretaceous stratigraphy

The Cretaceous deposits in the Jianghan Basin can be divided into two units, of the Early and Late Cretaceous age, respectively, representing two independent fining-upward cycles (Figs. 5, 6). Although the subdivisions of the two units vary across the Jianghan Basin, an appropriate uniform stratigraphic framework has been established (Fig. 6; HBGMR, 1990; Wang et al., 2014) based on the biostratigraphic data (Table 1, Lei et al., 1987; HBGMR, 1990), sedimentary cycle, stratigraphic contact relationship and detrital zircon U-Pb ages (constraining on the maximum depositional age, Shen et al., 2012a).

The Lower Cretaceous deposits unconformably overlie the pre-rift basement above an unconformity (Fig. 5A), with a maximum thickness of ~2000 m (Fig. 3). It shows a fining upward cycle and mainly consists of conglomerates and sandstone in the lower part and sandstone and siltstone in the upper part (Fig. 6). The sedimentary facies association of the Lower Cretaceous strata corresponds to alluvial fan and braided river (Li et al., 2006). The Upper Cretaceous strata lie conformably above the Lower Cretaceous strata (Fig. 5C; HBGMR, 1990; Wang et al., 2013a) and are up to ~4500 m thick. The observed thickness variation in this stratigraphic unit is mainly controlled by normal faults (Fig. 5F). At the basin margin, the Lower Cretaceous deposits mainly include conglomerates in the lower part, sandstones in the middle part and sandy mudstones and sandstones in the upper part (Figs. 5C, D, E and 6). Similar sedimentary cycle in the inner Jianghan

Basin was revealed by borehole data (Fig. 6). In general, seismic facies of the Upper Cretaceous deposits are characterized by low to medium amplitude, medium to high frequency and chaotic to continuous reflections (Figs. A2 and A3), which is consistent with the observed sedimentology. Moreover, the Hai9 well encountered more than 100 m thick basalt layers, indicating volcanism during the Late Cretaceous. In total, ten wells have encountered the basalt layers in the Upper Cretaceous strata as well as outcrops in the northeast basin, while they are absent in the Lower Cretaceous strata. The sedimentary environment during the Late Cretaceous included alluvial fan, braided river and shallow lake (Li et al., 2006).

4.2. Early Cretaceous basin architecture

Based on the available seismic and borehole data (Fig. 4) as well as previous studies (CM, 1970; YM, 1970, 1976; HBGMR, 1990), the distribution of the Lower Cretaceous deposits of the Jianghan Basin was defined (Figs. 6, 7). The mapping reveals that the Lower Cretaceous strata were absent in most of the Jianghan Basin and merely distributed at the basin margin. In the northwest corner of the Jianghan Basin (Fig. 7B), the Lower Cretaceous deposits have a maximum thickness of ~2000 m. They thicken southwest-ward (HBGMR, 1990), probably due to the uplift of the Huangling Massif (Ji et al., 2014) and its denudation. The distribution of the Lower Cretaceous strata is more limited in the northeastern corner (Fig. 7C), with a maximum thickness of 879 m (HBGMR, 1990). The Lower Cretaceous strata in these two regions pinch out towards the centre of the basin and is absent in most regions of the Jianghan Basin (Figs. 6, 7; HBGMR, 1990; Li et al., 2006; Liu et al., 2013).

The Tianyangping Fault dips towards the south-west and has a reverse sense of movement in the present day, although variations in sediment thickness across it reveals that it had a normal sense of offset during the Late Cretaceous to Paleogene and then underwent subsequent structural inversion (CM, 1970). In this study we infer from the thickness maps that the small population of normal faults in Fig. 7B and C initiated during the Late Cretaceous and were not active during the Early Cretaceous. Hence, the geometry of the Lower Cretaceous stratigraphic successions suggests a set of saucer-shaped depression sequences, showing an angular unconformity with underlying pre-rift strata and a conformable contact with the overlying Late Cretaceous deposits (Fig. 7D).

4.3. Late Cretaceous rifting characteristics

To constrain the Late Cretaceous rifting evolution of the Jianghan Basin, we present and analyse structural and stratal thickness maps and key cross sections (Fig. 8). The basin is divided into three domains based on the strike orientation of the principal faults (Fig. 8A).

4.3.1. North Jianghan Basin

The north Jianghan Basin is primarily controlled by the Tongchenghe, Yuan'an, Jingmen, Hanshui and Songhezhen faults, forming a series of NNW-trending grabens and half-grabens (Fig. 8 A). Most faults dip eastwards, while the Yuan'an and Tianyangping faults are two exceptions, with west and northeast dips respectively. The structural framework of the north basin crops out at the surface and is clearly evident in the geological map (Fig. 2), which shows a close correspondence between thrusts and folds exposed on the surface (HBGMR, 1990). Fig. 9 shows two structural cross sections across the north Jianghan Basin, presenting typical graben and half-graben geometry. In addition, the degree of deformation within the pre-rift basement reduces from east to west (section A-A' to section B-B'), suggesting that compression was from the east. The Hanshui Fault, the northern segment of which is shown in Fig. 10A, dips at 19° and is a low-angle normal fault, although its footwall may have rotated slightly. The pre-rift strata, derived from borehole penetrations, in the hanging wall of the Hanshui Fault are older than that in the footwall and become progressively older while approaching the fault plane. Hence as the Hanshui Fault juxtaposes older strata onto younger strata the fault has to have a compressional offset that was subsequently partly structurally inverted with a normal offset and reversed during the Late Cretaceous. This reflection section (Fig. 10A) is geometrically akin to the balanced cross-sections of reactivated fold and thrust belts, such as the northern Alpine foreland (Malz et al., 2016) and the Cape Fold Belt (Paton et al., 2006). Therefore, it seems likely that the Hanshui Fault has reactivated a compressional unroofed fault-related fold. However, the present anticline in the footwall of the Hanshui fault may largely result from the rotation of the pre-rift basement (hanging wall of the Jingmen Fault) during the syn-rift stage. In addition, some thrust faults preserved in the pre-rift basement (Fig. 10A).

4.3.2. Central Jianghan Basin

The central basin has a very complex fault system that is radially striking, generating a series of isolated grabens and half-grabens with multiple orientations (Fig. 8). The Jingmen and Hanshui faults extended from the basin margins into the central basin. The seismic section across the southern segment of the Hanshui Fault (Fig. 10B) shows an asymmetrical graben controlled by NE dipping Hanshui Fault and southwest dipping Zhugentan Fault (Fig. 8A). The Hanshui Fault dipping at 28° is a low-angle normal fault and seismic data reveal that pre-rift strata become progressively older with proximity to the fault plane. Pre-rift basement reflections in the footwall are difficult to correlate with the stratigraphy and we tentatively infer that strata at the top of the pre-rift basement are the Middle Triassic to Jurassic rocks based on nearby seismic-well ties. In addition, the

Zhugentan Fault is also likely to be a reactivated fault given the presence of older pre-rift strata in the hanging wall compared to the footwall.

The Wen'ansi and Wancheng faults (Figs. 8A, 10C) are two approximately NE-striking listric faults, ~38 and 55 km in length, respectively. The Wancheng Fault dipping at about 50° in the upper part controlled a large depocentre with a maximum thickness of ~4500 m (Fig. 8B), while the Wen'ansi Fault with 40° average dip in the upper part indicates a low cumulative displacement (Fig. 10C). The section across the Wen'ansi and Wancheng faults (Fig. 10C) shows similar characteristics of pre-rift basement to the sections across the Hanshui Fault (Fig. 10A, B), with pre-rift strata near the fault plane in the hanging wall being older than that in the footwall in both faults. Moreover, the basement strata in the hanging wall become progressively older with increasing proximity to the fault planes, indicating a reactivation of unroofed fault-related folds.

A low-angle normal fault zone is shown in Fig. 11A. The lower part of the fault is gently curving upward probably due to the uplift of the south Jianghan Basin at the end of syn-rift stage. The Upper Cretaceous strata were rotated to a dip of ca. 35°, which may result from the horizontal fault plane geometry at depth and intensive faulting during the Early Paleogene. Basement reflections are well defined in the footwall while poorly imaged in the hanging wall. The dominant southerly dip direction is consistent with the approximately north-directed thrusting of the Jiangnan Orogen. The Tianmenhe Fault has a listric geometry and dips at 40° in its upper part (Fig. 11B), flattening to ca. 10° dip at depth. The footwall area displays some basement reflections with limited coherency, while basement reflections in the hanging wall are high amplitude, continuous events making them easier to map (Fig. 11B). The well penetrating basement encountered the top of Devonian to Lower Triassic strata, which are younger than the strata near the fault plane in the hanging wall basement. The same relationship is evident with other major faults described above, the basement strata in the hanging wall of the Tianmenhe Fault also become progressively older while approaching the fault plane. This is likely to be a consequence of the unroofing of a fault-related fold before rifting initiated.

4.3.3. South Jianghan Basin

Overall, the south Jianghan Basin forms a northward dipping slope. A series of NE, nearly E-W and NW-striking faults developed within the slope, dipping southeast to southwest. These faults have generated a series of half-grabens that exhibit thinning of syn-rift stratigraphic successions towards the south (Fig. 8A and B). The Datonghu Fault, which is a listric fault, dips at 65° in the upper part (Fig. 11C). The southeast dipping Chahekou Fault, although shorter than the Datonghu Fault, shows higher activity during the Late Cretaceous. The pre-rift basement strata in the hanging wall and footwall show similar characteristics with the faults described above, suggesting a reactivation of an unroofed fault-related fold.

4.3.4. Summary of Late Cretaceous rifting characteristics

The characteristics of the Late Cretaceous rifting in the Jianghan Basin can be summarized as follows: (a) Major faults are radially striking, indicating a distributed, transtensional stress system or multi-directional extension during the Late Cretaceous; (b) depocentres are distributed with multiple orientations and the maximum subsidence was focused in the central Jianghan Basin; (c) a common feature of the major faults is that pre-rift basement strata in the hanging wall are older than that in the footwall and become progressively older as proximity to the fault plane increases. In some cases, pre-rift basement reflections are uncertain in the footwall, and tentative inferences are made based on the seismic and/or drilling data collected nearby (e. g., Figs. 10B and 11A), which suggests that these faults have reactivated pre-existing unroofed fault-related folds.

5. Discussion

5.1 The nature of the Early Cretaceous extension in the Jianghan Basin

The Jianghan Basin is one of a number of- extensional basins situated within the South China Block (e.g., Li et al., 2012b; Zhang et al., 2012). It has been demonstrated that the crustal contraction in the South China Block was terminated by intense crustal extension during the Early Cretaceous (Li, 2000; Li et al., 2014b). Li et al. (2014b) proposed that rifting began in the South China Block during the Early Cretaceous and the deposition of the Cretaceous strata expanded progressively eastward, with their depocentres shifting from inland in the Early Cretaceous to the coastal area in the Late Cretaceous (Fig. 12A). In addition, Cretaceous magmatic activity becomes younger progressively towards the southeast, hence migrates in a similar manner to the Cretaceous sedimentation from inland to the coastal areas (Li, 2000; Zhou and Li, 2000; Li et al., 2014b). The evolution of the Jianghan Basin (Section 4.2-4.3), therefore, can be considered as being relatively independent from the rest of the South China Block during the Cretaceous.

In the present day, the lithosphere to the west of NSGL has a typical thickness of approximately 180 km, but is only ~80 km to the east of NSGL (Zhou et al., 2012; Zheng et al., 2014; Li et al., 2015). The significant difference in lithospheric thickness resulted from rapid thinning due to the flat-slab subduction and rollback of the Pacific plate during the Mesozoic (Li and Li, 2007; Zhou et al., 2012; Li et al., 2015). The thinning of the previously overthickened lithosphere (more than 100 km) may have been necessary for rift initiation (e. g., Rooney et al., 2013) as continental lithosphere thicker than 100 km probably cannot magmatically rift (Bialas et al., 2010; Van Avendonk et al., 2015). Since most regions of the South China Block began to rift during the Early Cretaceous, the lithosphere in these areas must have been thinned to less than 100 km before the Early Cretaceous. This lithospheric thinning was largely with a consequence of the multiple phases of Triassic to Jurassic subduction of the Pacific plate and associated magmatism (Fig. 12B; Zhou et al., 2006; Li et al., 2012c). These phases of subduction resulted in hydration, weakening and thinning the lithospheric mantle under the South China Block. A similar situation also occurred in the North China Craton (Windley et al., 2010). However, during this period, the Jianghan Basin was located in a relatively stable foreland setting with no magmatism (Fig. 3), so there is no evidence that thinning of the lithosphere occurred. Since the Late Cretaceous intense rifting indicates that the thickness of lithosphere beneath the Jianghan Basin was already less than 100 km at that time, the lithosphere must have undergone rapid thinning during the Early Cretaceous.

The Huarong granitoids with emplacement ages at ca. 129 Ma and ca. 117 Ma (Fig. 2; Wang et al., 2008; Shen et al., 2012b; Ji et al., 2017a) provide evidence of the Early Cretaceous magmatism in the Jianghan Basin. Although no intruding dykes have been observed on seismic sections (Figs. 10 and 11), large-scale intrusion of mafic dykes into the lower crust was revealed from seismic wide-angle-reflection data (Zhang et al., 2009). We infer that either the intruding dykes were deeply buried and do not penetrate the surface, or they are too small in size and/or too steep in dip to identify on seismic sections.

During lithospheric thinning, a set of the Lower Cretaceous depression sequences were deposited in a restricted location on the basin margin while being absent in the rest of the basin. This geometry of syn-extensional basin fill does not fit the typical rift initiation model (Prosser, 1993; Cowie, 1998; Gupta et al., 1998; Gawthorpe and Leeder, 2000; Cowie et al., 2005). These observations conform to the active rifting model in which thermal doming is associated with magmatism within the central basin (Sengor and Burke, 1978; Corti et al., 2003; Ziegler and Cloetingh, 2004) and deposition at the basin margin (Nottvedt et al., 1995; Avni et al., 2012) prior to fault controlled rifting initiation. This suggests that thermal doming may have affected most areas of the Jianghan Basin during the lithospheric thinning in Early Cretaceous times. Contemporaneously, deposits passively filled in the space between the dome and surrounding topographic highs (orogens and massif). These depression sequences on the basin margin were referred to as "Proto-rift units" by Nottvedt et al. (1995), which have tabular depositional architectures and are mostly conformably overlain by syn-rift deposits. These characteristics have a good correspondence with the Lower Cretaceous deposits in the Jianghan Basin (Fig. 7).

5.2 How did Late Cretaceous faults with radial strikes develop?

The structural analysis presented in section 4.3 suggests that the Late Cretaceous major normal faults resulted from the reactivation of pre-existing thrusts, therefore their strikes suggest the orientations of pre-existing structures. Together with the regional geological data, we present a framework of the pre-existing structures (Fig. 13) that illustrates the deformation and structural division of the pre-rift basement in Jianghan area.

During the Late Jurassic, as the Southern Qinling-Dabie Thrust Belt propagated southwest-ward and the Northern Jiangnan Thrust Belt propagated northwards (Liu et al., 2015), with the obstruction of the Huangling Massif, three structural belts formed with distinct characteristics (Fig. 13). The Southern Qinling-Dabie Thrust Belt was arc-shaped due to the obstruction of the Huangling Massif and nearly E-W-striking linear-shaped Northern Jiangnan Thrust Belt. Contemporaneously, a ring-shaped structural belt formed surrounding the oval-shaped Huangling Massif. These three belts overlapped one another, forming an interfering and converging zone between them (Mei et al., 2008; Liu et al., 2015). As the thrust directions in the Southern Qinling-Dabie Thrust Belt and Northern Jiangnan Thrust Belt were oblique to each other, some thrust faults in the interfering and converging zone are likely to have strike-slip component (Guo et al., 2007) and some degree of transpression.

As a result, pre-existing structures in the north Jianghan Basin predominantly have a NNW-strike while they were approximately EW-striking in the south Jianghan Basin. The central Jianghan Basin is located in the interfering and converging zone, as a consequence of which is that its pre-existing structures are radially striking. Even so, how did these pre-existing structures synchronously undergo extensional reactivation during Late Cretaceous rifting? Apparently, it is unlikely the result of regional extension in a uniform direction (e.g., Late Cretaceous N-S extension in the South China Block, Li et al., 2014b), which however is a common phenomenon in many rift basins, such as Baikal rift (Philippon et al., 2015) and East African rift system (Morley 2010; Acocella, 2014; Philippon et al., 2015). We propose that it resulted from the mantle upwelling (cf. Qi and Yang, 2010). During the Late Cretaceous, driven by the continued upwelling of asthenospheric mantle, the pre-existing thrusts with radial strikes simultaneously reactivated as normal faults, forming a number of distributed grabens and half-grabens with multiple orientations (Fig. 8A). In addition, as the central Jianghan Basin was located in the interfering and converging zone, it underwent more intense and complex thrusting and folding during the Late Jurassic than the north and south basins, consequently becoming much weaker and therefore easier to rift. This resulted in the maximum subsidence being focused in the central Jianghan Basin.

5.3 Initial rifting processes of the Jianghan Basin

Based on our observations, we present a conceptual model for the initial rifting processes of the Jianghan Basin (Fig. 14) that illustrates how Cretaceous tectonics switched from compression to extension.

By the latest Jurassic, the pre-rift basement strata underwent thrusting and folding due to the compression of the Qinling-Dabie Orogenic Belt and Jiangnan Orogen and the obstruction of the Huangling Massif (Fig. 14A; Liu et al., 2015). Contemporaneously, the lithosphere beneath most of the South China Block was thinned to < 100 km after the Triassic to Jurassic hydrating, weakening and thinning phases (See Section 5.1). During the Early Cretaceous, while the large-scale roll-back of the subducted Pacific slab (Yang et al., 2012, 2014; Li et al., 2014b) triggered unsteady mantle flow (Fig. 14B), dehydration of the stagnant subducting (Niu, 2005; Huang and Zhao, 2006) Pacific slab weakened the upper mantle (Zheng et al., 2008), significantly facilitating erosion of the lithospheric mantle (Fig. 14B; Niu, 2005). Furthermore, the hot upwelling asthenospheric material intruded into the lithosphere beneath the Jianghan basin heating and weakening the lithosphere (Bialas et al., 2010), leading to thermal doming of most of the Jianghan Basin. However, on the basin margin, which was relatively unaffected by the thermal doming event, a set of localized depression sequences were deposited. During the Early Cretaceous, rifting initiated in most of the South China Block. As the lithosphere beneath the Jianghan Basin was thinned to less than 100 km by the end of the Early Cretaceous, the basin began to rift during the Late Cretaceous under the diapirism of the continuously upwelling mantle and magma (Fig. 14C). The pre-existing thrusts with radial strikes simultaneously underwent extensional reactivation, forming a series of normal faults with multiple orientations. The maximum subsidence was focused in the central Jianghan Basin, as it was located in the interfering and converging zone between the two orogenic belts, and thus its pre-rift basement was weaker than the north and south basins.

6. Conclusion

Using an extensive database of geological and geophysical data, we present a new model to answer when and how rifting initiated in the Jianghan Basin. The tectonic switch from thrusting and folding to rifting in the Jianghan Basin can be divided into two distinct stages based on the stratigraphic and structural record and the comprehensive comparison with the tectonic evolution of the South China Block. During the Early Cretaceous, the Jianghan Basin was characterized by lithospheric thinning, thermal doming and local depression. This process was triggered by the large-scale roll-back of the subducted Pacific slab. Unsteady mantle flow coupled with dehydration of the stagnant subducting Pacific slab made the lithosphere beneath the Jianghan Basin rapidly thinned. The hot upwelling asthenospheric material and intruded dykes/magma heated and weakened the lithosphere, leading to thermal doming of most of the Jianghan Basin. Meanwhile, on the basin margin, which was relatively unaffected by the thermal doming event, a set of localized depression sequences were deposited. During the Late Cretaceous, the lithosphere was already thin enough (less than 100 km) to rift. Under the diapirism of the continuously upwelling asthenospheric mantle, the pre-existing thrusts with radial strikes simultaneously reactivated, forming a series of normal faults with multiple orientations. Since the central Jianghan Basin is located in the interfering and converging zone between surrounding orogens and underwent more intense thrusting and folding than the north and south basins, it become much weaker and therefore easier to rift, focusing the maximum subsidence. This paper provides detailed stratigraphic and structural evidence for active rifting model and illustrates its initiation processes.

Acknowledgments

We are grateful to Dr. Marcin Machalski and an anonymous reviewer for their constructive comments and suggestions. This work was financially supported by the Natural Science Foundation of Hubei Province (2016CFA084), the Major National Science and Technology Programs, China (2016ZX05002-006) and the Scientific Research Project of China Petroleum and Chemical Corporation (P14111).

Appendix A. Supplementary material

Fig. A1 Images of pre-rift basement reflections and interpretion based on seismic-well ties and depth-conversion. See Fig. 4 for location.

Fig. A2 Uninterpreted seismic sections across the Hanshui Fault (A, B), Wen’ansi Fault and Wancheng Faults (C). See Figs. 4 and 8A for location.

Fig. A3 Uninterpreted seismic sections across the Zibei Fault Zone (A), Tianmenhe Fault (B) and Datonghu Fault (C). See Figs. 4 and 8A for location.

References

Acocella, V., 2014. Structural control on magmatism along divergent and convergent plate boundaries: Overview, model, problems. Earth-Science Reviews 136, 226-288. DOI: 10.1016/j.earscirev.2014.05.006.

Amante, C., B.W. Eakins, 2009. ETOPO1 1 Arc-Minute Global Relief Model: Procedures, Data Sources and Analysis. NOAA Technical Memorandum NESDIS NGDC-24. National Geophysical Data Center, NOAA. DOI: 10.7289/V5C8276M.

Avni, Y., Segev, A., Ginat, H., 2012. Oligocene regional denudation of the northern Afar dome: Pre- and syn-breakup stages of the Afro-Arabian plate. Geological Society of America Bulletin 124(11-12), 1871-1897. DOI: 10.1130/B30634.1.

Bell, R.E., Jackson, C.A.L., Whipp, P.S., Clements, B., 2014. Strain migration during multiphase extension: Observations from the northern North Sea. Tectonics 33, 1936-1963. DOI: 10.1002/2014TC003551.

Bialas, R.W., Buck, W.R., Qin, R., 2010. How much magma is required to rift a continent? Earth and Planetary Science Letters 292, 68-78. DOI: 10.1016/j.epsl.2010.01.021.

Buiter, S.J.H., Torsvik, T.H., 2014. A review of Wilson Cycle plate margins: A role for mantle plumes in continental break-up along sutures? Gondwana Research 26(2), 627-653. DOI: 10.1016/j.gr.2014.02.007.

Chen, L., Ma, C., She, Z., Mason, R., Zhang, J., Zhang, C., 2009. Petrogenesis and tectonic implications of A-type granites in the Dabie orogenic belt, China: geochronological and geochemical constraints. Geological Magazine 146, 638-651. DOI: 10.1017/S0016756808005918.

CM (Changyang Map), 1970. 1:200 000 Geological Map of the People’s Republic of China, Changyang Region (in Chinese).

Corti, G., Bonini, M., Conticelli, S., Innocenti, F., Manetti, P., Sokoutis, D., 2003. Analogue modelling of continental extension: a review focused on the relations between the patterns of deformation and the presence of magma. Earth-Science Reviews 63, 169-247. DOI: 10.1016/S0012-8252(03)00035-7.

Cowie, P.A., Underhill, J.R., Behn, M.D., Lin, J., Gill, C.E., 2005. Spatio-temporal evolution of strain accumulation derived from multi-scale observations of Late Jurassic rifting in the northern North Sea: A critical test of models for lithospheric extension. Earth and Planetary Science Letters 234, 401-419. DOI: 10.1016/j.epsl.2005.01.039.

Cowie, P.A., 1998. A healing–reloading feedback control on the growth rate of seismogenic faults. Journal of Structural Geology 20, 1075-1087. DOI: 10.1016/S0191-8141(98)00034-0.

Dong, Y., Zhang, G., Neubauer, F., Liu, X., Genser, J., Hauzenberger, C., 2011. Tectonic evolution of the Qinling orogen, China: Review and synthesis. Journal of Asian Earth Sciences 41, 213-237. DOI: 10.1016/j.jseaes.2011.03.002.

Ford, M., Rohais, S., Williams, E.A., Bourlange, S., Jousselin, D., Backert, N., Malartre, F., 2013. Tectono-sedimentary evolution of the western Corinth rift (Central Greece). Basin Research 25, 3-25. DOI: 10.1111/j.1365-2117.2012.00550.x.

Frey, H.M., Lange, R.A., Hall, C.M., Delgado-Granados, H., Carmichael, I.S.E., 2007. A Pliocene ignimbrite flare-up along the Tepic-Zacoalco rift: Evidence for the initial stages of rifting between the Jalisco block (Mexico) and North America. Geological Society of America Bulletin 119(1-2), 49-64. DOI: 10.1130/B25950.1.

Gawthorpe, R.L., Jackson, C., Young, M.J., Sharp, I.R., Moustafa, A.R., Leppard, C.W., 2003. Normal fault growth, displacement localisation and the evolution of normal fault populations: the Hammam Faraun fault block, Suez rift, Egypt. Journal of Structural Geology 25, 883-895. DOI: 10.1016/S0191-8141(02)00088-3.

Gawthorpe, R.L., Leeder, M.R., 2000. Tectono-sedimentary evolution of active extensional basins. Basin Research 12, 195-218. DOI: 10.1046/j.1365-2117.2000.00121.x.

Gong, H., 2014. Tectonic evolution and its control on coal-measure source rocks in Zhu-3 depression of Pearl River Mouth Basin. Master's Thesis, China University of Mining and Technology, Xuzhou (in Chinese with English abstract).

Gouiza, M., Hall, J., Bertotti, G., 2015. Rifting and pre-rift lithosphere variability in the Orphan Basin, Newfoundland margin, Eastern Canada. Basin Research 27, 367-386. DOI: 10.1111/bre.12078.

Guo, P., Niu, Y., Ye, L., Liu, J., Sun, P., Cui, H., Zhang, Y., Gao, J., Su, L., Zhao, J., Feng, Y., 2014. Lithosphere thinning beneath west North China Craton: Evidence from geochemical and Sr–Nd–Hf isotope compositions of Jining basalts. Lithos 202, 37-54. DOI: 10.1016/j.lithos.2014.04.024.

Guo, Z., Liu, X., Chen, H., 2007. Basin-mountain coupling relationship and oil-gas response in lower Palaeozoic since the Indo-China epoch in Jianghan Basin. Petroleum Geology and Recovery efficiency 14, 49-51 (in Chinese with English abstract).

Gupta, S., Cowie, P.A., Dawers, N.H., Underhill, J.R., 1998. A mechanism to explain rift-basin subsidence and stratigraphic patterns through fault-array evolution. Geology 26, 595. DOI: 10.1130/0091-7613(1998)026<0595:AMTERB>2.3.CO;2.

HBGMR (Henan Bureau of Geology and Mineral Resources), 1989. Regional Geology of the Henan Province. Geological Press, Beijing (in Chinese with English summary).

HBGMR (Hubei Bureau of Geology and Mineral Resources), 1990. Regional Geology of the Hubei Province. Geological Press, Beijing (in Chinese with English summary).

HBGMR (Hunan Bureau of Geology and Mineral Resources), 1988. Regional Geology of the Hunan Province. Geological Press, Beijing (in Chinese with English summary).

Henstra, G.A., Gawthorpe, R.L., Helland-Hansen, W., Ravnas, R., Rotevatn, A., 2016. Depositional systems in multiphase rifts: seismic case study from the Lofoten margin, Norway. Basin Research 28, 1-23. DOI: 10.1111/bre.12183.

Henstra, G.A., Rotevatn, A., Gawthorpe, R.L., Ravnas, R., 2015. Evolution of a major segmented normal fault during multiphase rifting: The origin of plan-view zigzag geometry. Journal of Structural Geology 74, 45-63. DOI: 10.1016/j.jsg.2015.02.005.

Huang, J. and Zhao, D., 2006. High-resolution mantle tomography of China and surrounding regions. Journal of Geophysical Research-Solid Earth 111, B09305B9. DOI: 10.1029/2005JB004066.

Ji, W., Faure, M., Lin, W., Chen, Y., Chu, Y., Xue, Z., 2018. Multiple Emplacement and Exhumation History of the Late Mesozoic Dayunshan-Mufushan Batholith in Southeast China and Its Tectonic Significance: 1. Structural Analysis and Geochronological Constraints. Journal of Geophysical Research: Solid Earth 123(1), 689-710. DOI: 10.1002/2017JB014597.

Ji, W., Lin, W., Faure, M., Chen, Y., Chu, Y., Xue, Z., 2017a. Origin of the Late Jurassic to Early Cretaceous peraluminous granitoids in the northeastern Hunan province (middle Yangtze region), South China: Geodynamic implications for the Paleo-Pacific subduction. Journal of Asian Earth Sciences 141, 174-193. DOI: 10.1016/j.jseaes.2016.07.005.

Ji, W., Lin, W., Faure, M., Chu, Y., Wu, L., Wang, F., Wang, J., Wang, Q., 2014. Origin and tectonic significance of the Huangling massif within the Yangtze craton, South China. Journal of Asian Earth Sciences 86, 59-75. DOI: 10.1016/j.jseaes.2013.06.007.

Ji, W., Lin, W., Faure, M., Shi, Y., Wang, Q., 2017b. The early Cretaceous orogen-scale Dabieshan metamorphic core complex: implications for extensional collapse of the Triassic HP–UHP orogenic belt in east-central China. International Journal of Earth Sciences 106(4), 1311-1340. DOI: 10.1007/s00531-016-1311-6.

Lei Y., Guan, S., Zhang, Q., Sun, Q., 1987. Biostratigraphy of the Yangtze Gorge Area. Geological Publishing House, Beijing, pp. 28-33.

Li, J., Bi, S., Selby, D., Chen, L., Vasconcelos, P., Thiede, D., Zhou, M., Zhao, X., Li, Z., Qiu, H., 2012a. Giant Mesozoic gold provinces related to the destruction of the North China craton. Earth and Planetary Science Letters 349, 26-37. DOI: 10.1016/j.epsl.2012.06.058.

Li, J., Vasconcelos, P.M., Zhou, M., Deng, X., Cohen, B., Bi, S., Zhao, X., Selby, D., 2014a. Longevity of magmatic-hydrothermal systems in the Daye Cu-Fe-Au District, eastern China with implications for mineral exploration. Ore Geology Reviews 57, 375-392. DOI: 10.1016/j.oregeorev.2013.08.002.

Li, J., Zhang, Y., Dong, S., Johnston, S.T., 2014b. Cretaceous tectonic evolution of South China: A preliminary synthesis. Earth-Science Reviews 134, 98-136. DOI: 10.1016/j.earscirev.2014.03.008.

Li, J., Zhang, Y., Dong, S., Li, H., 2012b. Late Mesozoic-Early Cenozoic deformation history of the Yuanma Basin, central South China. Tectonophysics 570, 163-183. DOI: 10.1016/j.tecto.2012.08.012.

Li, J., Zhao, X., Zhou, M., Ma, C., de Souza, Z.S., Vasconcelos, P., 2009. Late Mesozoic magmatism from the Daye region, eastern China: U-Pb ages, petrogenesis, and geodynamic implications. Contributions to Mineralogy and Petrology 157, 383-409. DOI: 10.1007/s00410-008-0341-x.

Li, Q., Guo, J., Zeng, F., Duan, H., 2006. Cretaceous sedimentary facies and the evolution in

Jianghan Basin. Journal of Southwest Petroleum Institute 28, 5-8 (in Chinese with English abstract).

Li, X., 2000. Cretaceous magmatism and lithospheric extension in Southeast China. Journal of Asian Earth Sciences 18, 293-305. DOI: 10.1016/S1367-9120(99)00060-7.

Li, X., Zhu, P., Kusky, T.M., Gu, Y., Peng, S., Yuan, Y., Fu, J., 2015. Has the Yangtze craton lost its root? A comparison between the North China and Yangtze cratons. Tectonophysics 655, 1-14. DOI: 10.1016/j.tecto.2015.04.008.

Li, Z., Li, X., 2007. Formation of the 1300-km-wide intracontinental orogen and postorogenic magmatic province in Mesozoic South China: A flat-slab subduction model. Geology 35, 179-182. DOI: 10.1130/G23193A.1.

Li, Z., Li, X., Chung, S., Lo, C., Xu, X., Li, W., 2012c. Magmatic switch-on and switch-off along the South China continental margin since the Permian: Transition from an Andean-type to a Western Pacific-type plate boundary. Tectonophysics 532, 271-290. DOI: 10.1016/j.tecto.2012.02.011.

Liu, S., Heller, P.L., Zhang, G., 2003. Mesozoic basin development and tectonic evolution of the Dabieshan orogenic belt, central China. Tectonics 22, 10384. DOI: 10.1029/2002TC001390.

Liu, S., Li, W., Wang, K., Qian, T., Jiang, C., 2015. Late Mesozoic development of the southern Qinling-Dabieshan foreland fold-thrust belt, Central China, and its role in continent-continent collision. Tectonophysics 644, 220-234. DOI: 10.1016/j.tecto.2015.01.015.

Liu, S., Steel, R., Zhang, G., 2005. Mesozoic sedimentary basin development and tectonic implication, northern Yangtze Block, eastern China: record of continent - continent collision. Journal of Asian Earth Sciences 25, 9-27. DOI: 10.1016/j.jseaes.2004.01.010.

Liu, S., Zhang, G., 2013. Mesozoic basin development and its indication of collisional orogeny in the Dabie orogen. Chinese Science Bulletin 58, 827-852. DOI: 10.1007/s11434-012-5503-6.

Ma, X., 1989. Atlas of Lithospheric Dynamics of China. China Cartographic Publishing House, Beijing, China pp.1-70.

Malz, A., Madritsch, H., Meier, B., Kley, J., 2016. An unusual triangle zone in the external northern Alpine foreland (Switzerland): Structural inheritance, kinematics and implications for the development of the adjacent Jura fold-and-thrust belt. Tectonophysics 670, 127-143. DOI: 10.1016/j.tecto.2015.12.025.

Mei, L., Dai, S., Shen, C., Tang, J., 2008. Formation and disintegration of Mesozoic-Cenozoic intracontinental ramp zone in Middle and Lower Yangtze Region. Geological Science and Technology Information 27, 1-7 (in Chinese with English abstract).

Mei, L., Deng, D., Shen, C., Liu, Z., 2012. Tectonic dynamic and marine hydrocarbon accumulation of Jiangnan-Xufeng Uplift. Geological Science and Technology Information 31, 85-93 (in Chinese with English abstract).

Miller, N.C., Lizarralde, D., 2013. Thick evaporites and early rifting in the Guaymas Basin, Gulf of California. Geology 41(2), 283-286. DOI: 10.1130/G33747.1.

Mohammed, M., Paton, D., Collier, R.E.L., Hodgson, N., Negonga, M., 2017. Interaction of crustal heterogeneity and lithospheric processes in determining passive margin architecture on the southern Namibian margin. Geological Society, London, Special Publications 438(1), 177-193. DOI: 10.1144/SP438.9.

Morley, C.K., 2010. Stress re-orientation along zones of weak fabrics in rifts: An explanation for pure extension in ‘oblique’ rift segments? Earth and Planetary Science Letters 297(3-4), 667-673. DOI: 10.1016/j.epsl.2010.07.022.

Natali, C., Beccaluva, L., Bianchini, G., Siena, F., 2011. Rhyolites associated to Ethiopian CFB: Clues for initial rifting at the Afar plume axis. Earth and Planetary Science Letters 312, 59-68. DOI: 10.1016/j.epsl.2011.09.059.

Niu, Y., 2005. Generation and Evolution of Basaltic Magmas: Some Basic Concepts and a New View on the Origin of Mesozoic- Cenozoic Basaltic Volcanism in Eastern China. Geological journal of China universities 11, 9-46.

Nixon, C.W., McNeill, L.C., Bull, J.M., Bell, R.E., Gawthorpe, R.L., Henstock, T.J., Christodoulou, D., Ford, M., Taylor, B., Sakellariou, D., Ferentinos, G., Papatheodorou, G., Leeder, M.R., Collier, R.E.L.I., Goodliffe, A.M., Sachpazi, M., Kranis, H., 2016. Rapid spatiotemporal variations in rift structure during development of the Corinth Rift, central Greece. Tectonics 35, 1225-1248. DOI: 10.1002/2015TC004026.

NM (Nanzhang Map), 1965. 1:200 000 Geological Map of the People’s Republic of China, Nanzhang Region.

Nottvedt, A., Gabrielsen, R.H., Steel, R.J., 1995. Tectonostratigraphy and sedimentary architecture of rift basins, with reference to the northern North Sea. Marine and Petroleum Geology 12, 881-901. DOI: 10.1016/0264-8172(95)98853-W.

Omar, G.I., Steckler, M.S., 1995. Fission Track Evidence on the Initial Rifting of the Red Sea: Two Pulses, No Propagation. 270(5240), 1341 - 1344. DOI: 10.1126/science.270.5240.1341.

Paton, D.A., 2006. Influence of crustal heterogeneity on normal fault dimensions and evolution: southern South Africa extensional system. Journal of Structural Geology 28(5), 868-886. DOI: 10.1016/j.jsg.2006.01.006.

Paton, D.A., Macdonald, D.I.M., Underhill, J.R., 2006. Applicability of thin or thick skinned structural models in a region of multiple inversion episodes; southern South Africa. Journal of Structural Geology 28(11), 1933-1947. DOI: 10.1016/j.jsg.2006.07.002.

Peron-Pinvidic, G., Osmundsen, P.T., 2016. Architecture of the distal and outer domains of the Mid-Norwegian rifted margin: Insights from the Ran-Gjallar ridges system. Marine and Petroleum Geology 77, 280-299. DOI: 10.1016/j.marpetgeo.2016.06.014.

Philippon, M., Willingshofer, E., Sokoutis, D., Corti, G., Sani, F., Bonini, M., Cloetingh, S., 2015. Slip re-orientation in oblique rifts. Geology 43(2), 147-150. DOI: 10.1130/G36208.1.

Prosser, S., 1993. Rift-related linked depositional systems and their seismic expression. Geological Society, London, Special Publications 71, 35-66.

Putirka, K., Platt, B., 2012. Basin and Range volcanism as a passive response to extensional tectonics. Geosphere 8(6), 1274-1285. DOI: 10.1130/GES00803.1.

Qi, J., Yang, Q., 2010. Cenozoic structural deformation and dynamic processes of the Bohai Bay basin province, China. Marine and Petroleum Geology 27, 757-771. DOI:10.1016/j.marpetgeo.2009.08.012.

Qiao, Y., Shan, Y., Tian, Y., Nie, G., Sun, B., 2012. Macro-deformation mechanisms for the Cretaceous Yuanan Basin, Western Hubei, Central China. Geotectonica et Metallogenia 36, 44-55 (in Chinese with English abstract).

Rajchl, M., Ulicny, D., Grygar, R., Mach, K., 2009. Evolution of basin architecture in an incipient continental rift: the Cenozoic Most Basin, Eger Graben (Central Europe). Basin Research 21, 269-294. DOI: 10.1111/j.1365-2117.2008.00393.x.

Rohais, S., Eschard, R., Ford, M., Guillocheau, F., Moretti, I., 2007. Stratigraphic architecture of the Plio-Pleistocene infill of the Corinth Rift: Implications for its structural evolution. Tectonophysics 440, 5-28. DOI: 10.1016/j.tecto.2006.11.006.

Rooney, T.O., Mohr, P., Dosso, L., Hall, C., 2013. Geochemical evidence of mantle reservoir evolution during progressive rifting along the western Afar margin. Geochimica et Cosmochimica Acta 102, 65-88. DOI: 10.1016/j.gca.2012.08.019.

Sengor, A.M.C., Burke, K., 1978. Relative timing of rifting and volcanism on Earth and its tectonic implications. Geophysical Research Letters 5(6), 419-421. DOI: 10.1029/GL005i006p00419.

Shen, C., Donelick, R.A., O'Sullivan, P.B., Jonckheere, R., Yang, Z., She, Z., Miu, X., Ge, X., 2012a. Provenance and hinterland exhumation from LA-ICP-MS zircon U-Pb and fission-track double dating of Cretaceous sediments in the Jianghan Basin, Yangtze block, central China. Sedimentary Geology 281, 194-207. DOI: 10.1016/j.sedgeo.2012.09.009.

Shen, C., Mei, L., Min, K., Jonckheere, R., Ratschbacher, L., Yang, Z., Peng, L., Liu, Z., 2012b. Multi-chronometric dating of the Huarong granitoids from the middle Yangtze Craton: Implications for the tectonic evolution of eastern China. Journal of Asian Earth Sciences 52, 73-87. DOI: 10.1016/j.jseaes.2012.02.013.

Shi, W., Dong, S., Ratschbacher, L., Tian, M., Li, J., Wu, G., 2013. Meso-Cenozoic tectonic evolution of the Dangyang Basin, north-central Yangtze craton, central China. International Geology Review 55, 382-396. DOI: 10.1080/00206814.2012.715732.

Tian, M., Shi, W., Li, J., Qu, H., 2010. Tectonic deformation analysis and paleostress field sequence of the grabens in the northwestern Jianghan Basin. Acta Geologica Sinica 84, 159-170 (in Chinese with English abstract).

Van Avendonk, H.J.A., Christeson, G.L., Norton, L.O., Eddy, D.R., 2015. Continental rifting and sediment infill in the northwestern Gulf of Mexico. Geology 43(7), 631-634. Doi: 10.1130/G36798.

Wang, B., Chen, Y., Lu, G., Liu, J., 2006. Episodic tectonic movement and evolutional characteristics of the Jianghan Basin. Oil Geophysical Prospecting 41, 226-230 (in Chinese with English abstract).

Wang, P., Liu, S., Zheng, H., Wang, K., Gao, T., Pan, F., Li, W., Jiang, C., Chen, Y., Yang, X., 2013a. Late-orogenic arcuate fold-thrust belts in northern Yangtze area: Structural characteristics and basin evolution. Journal of Palaeogeography 15, 819-838 (in Chinese with English abstract).

Wang, P., Mattern, F., Didenko, N.A., Zhu, D., Singer, B., Sun, X., 2016. Tectonics and cycle system of the Cretaceous Songliao Basin: An inverted active continental margin basin. Earth-Science Reviews 159, 82-102. DOI: 10.1016/j.earscirev.2016.05.004.

Wang, P., Zheng, H., Chen, L., Chen, J., Xu, Y., Wei, X., Yao, X., 2014. Exhumation of the Huangling anticline in the Three Gorges region: Cenozoic sedimentary record from the western Jianghan Basin, China. Basin Research 26, 505-522. DOI: 10.1111/bre.12047.

Wang, L., Ma, C., Zhang, J., Chen, L., Zhang, C., 2008. Petrological and geochemical characteristics and petrogenesis of the Early Cretaceous Taohuashan-Xiaomoshan Granites in northeastern Hunan Province. Geological Journal of China Universities 14(3), 334-349 (in Chinese with English abstract).

Wang, Y., Fan, W., Zhang, G., Zhang, Y., 2013b. Phanerozoic tectonics of the South China Block: Key observations and controversies. Gondwana Research 23, 1273-1305. DOI: 10.1016/j.gr.2012.02.019.

Wilson, J.T., 1966. Did the Atlantic close and then re-open? Nature 211(5050), 676-681. DOI: 10.1038/211676a0.

Windley, B.F., Maruyama, S., Xiao, W.J., 2010. Delamination thinning of subcontinental lithospheric mantle under Eastern China: The role of water and multiple subduction. American Journal of Science 310, 1250-1293. DOI: 10.2475/10.2010.03.

Xie, G., Mao, J., Li, X., Duan, C., Yao, L., 2011. Late Mesozoic bimodal volcanic rocks in the Jinniu basin, Middle-Lower Yangtze River Belt (YRB), East China: Age, petrogenesis and tectonic implications. Lithos 127, 144-164. DOI: 10.1016/j.lithos.2011.08.012.

Yang, S., Jiang, S., Zhao, K., Jiang, Y., Ling, H., Luo, L., 2012. Geochronology, geochemistry and tectonic significance of two Early Cretaceous A-type granites in the Gan-Hang Belt, Southeast China. Lithos 150, 155-170. DOI: 10.1016/j.lithos.2012.01.028.

Yang, Y., Chen, F., Siebel, W., Zhang, H., Long, Q., He, J., Hou, Z., Zhu, X., 2014. Age and composition of Cu-Au related rocks from the lower Yangtze River belt: Constraints on paleo-Pacific slab roll-back beneath eastern China. Lithos 202, 331-346. DOI: 10.1016/j.lithos.2014.06.007.

Yao, W., Li, Z., Li, W., Su, L., Yang, J., 2015. Detrital provenance evolution of the Ediacaran-Silurian Nanhua foreland basin, South China. Gondwana Research 28, 1449-1465. DOI: 10.1016/j.gr.2014.10.018.

YM (Yichang Map), 1970. 1:200 000 Geological Map of the People's Republic of China, Yichang Region (in Chinese).

YM (Yicheng Map), 1965. 1:200 000 Geological Map of the People's Republic of China, Yicheng Region.

YM (Yingcheng Map), 1976. 1:200 000 Geological Map of the People's Republic of China, Yingcheng Region (in Chinese).

Yu, Y., Gao, S.S., Moidaki, M., Reed, C.A., Liu, K.H., 2015. Seismic anisotropy beneath the incipient Okavango rift: Implications for rifting initiation. Earth and Planetary Science Letters 430, 1-8. DOI: 10.1016/j.epsl.2015.08.009.

Zhang, Y., Dong, S., Li, J., Cui, J., Shi, W., Su, J., Li, Y., 2012. The new progress in the study of Mesozoic tectonics of South China. Acta Geoscientica Sinica 33, 257-279 (in Chinese with English abstract).

Zhang, Z., Bai, Z., Mooney, W., Wang, C., Chen, X., Wang, E., Teng, J., Okaya, N., 2009. Crustal structure across the Three Gorges area of the Yangtze platform, central China, from seismic refraction/wide-angle reflection data. Tectonophysics 475, 423-437. DOI: 10.1016/j.tecto.2009.05.022.

Zheng, T., Zhao, L., He, Y., Zhu, R., 2014. Seismic imaging of crustal reworking and lithospheric modification in eastern China. Geophysical journal International 196, 656-670. DOI: 10.1093/gji/ggt420.

Zheng, T., Zhao, L., Zhu, R., 2008. Insight into the geodynamics of cratonic reactivation from seismic analysis of the crust-mantle boundary. Geophysical Research Letters 35, L083038. DOI: 10.1029/2008GL033439.

Zhou, L., Xie, J., Shen, W., Zheng, Y., Yang, Y., Shi, H., Ritzwoller, M.H., 2012. The structure of the crust and uppermost mantle beneath South China from ambient noise and earthquake tomography. Geophysical journal International 189, 1565-1583. DOI: 10.1111/j.1365-246X.2012.05423.x.

Zhou, X., Li, W., 2000. Origin of Late Mesozoic igneous rocks in Southeastern China: implications for lithosphere subduction and underplating of mafic magmas. Tectonophysics 326, 269-287. DOI: 10.1016/S0040-1951(00)00120-7.

Zhou, X., Sun, T., Shen, W., Shu, L., Niu, Y., 2006. Petrogenesis of Mesozoic granitoids and volcanic rocks in South China: A response to tectonic evolution. Episodes 29, 26-33.

Zhu, R., Fan, H., Li, J., Meng, Q., Li, S., Zeng, Q., 2015. Decratonic gold deposits. Science China-Earth Sciences 58, 1523-1537. DOI: 10.1007/s11430-015-5139-x.

Ziegler, P.A., Cloetingh, S., 2004. Dynamic processes controlling evolution of rifted basins. Earth-Science Reviews 64(1-2), 1-50. DOI: 10.1016/S0012-8252(03)00041-2.

ZM (Zhongxiang Map), 1976. 1:200 000 Geological Map of the People’s Republic of China, Zhongxiang Region.

Figure captions

Fig. 1. (A) Simplified map showing the topography and tectonic divisions of eastern Asia. (B) Vertical section of P wave velocity perturbations across the western Pacific-eastern China at the latitude 30ºN (after Huang and Zhao, 2006), showing the Pacific slab lying horizontally in the mantle transition zone (MTZ). Topography map is based on Etopo 1 (Amante and Eakins, 2009). Tectonic divisions are modified from Li and Li (2007), Mei et al. (2012), Zhu et al. (2015). NSGL,

North-South Gravity Lineament (modified from Ma, 1989).

Fig. 2. Geological map of the Jianghan basin and adjacent areas, modified after HBGMR, 1988, 1989, 1990. See Fig. 1A for location.

Fig. 3. Tectonostratigraphic chart for the Jianghan Basin showing the lithostratigraphy, basin evolution and main regional events (modified from HBGMR, 1988, 1989, 1990; Dong et al., 2011; Wang et al., 2013b; Li et al., 2014b; Yao et al., 2015). SCB, South China Block; NCC, North China Craton. The term "Proto-rift" is from Nottvedt et al. (1995). The Sinian in the Chinese literatures is equivalent to the Ediacaran.

Fig. 4. Map showing the coverage of 2-D and 3-D seismic reflection data and drilling wells penetrating the Upper Cretaceous strata and /or pre-rift basement, along with two structural cross sections and main field observation points. Wells marked by blue, red and dark dots are shown in Figs. 6, 10-11 and A1, respectively.

Fig. 5. Outcrop photos of the Cretaceous in the Jianghan Basin. A, Shimen Formation, grey conglomerate unconformably overlying Ordovician dolomite; B, Wulong Formation, grey sandstone with interbedded brick-red mudstone; C, conformable contact between Luojingtan Formation (grey conglomerate) and Wulong Formation (grey sandstone and conglomerate with interbedded brick-red mudstone); D, Honghuatao Formation, brick-red sandstone; E, Paomagang Formation, brown-red mudstone with interbedded grey-green siltstone and sandstone; F, Jingmen

Fault, purple-red sandstone of Paomagang Formation in the hanging wall and grey-white limestone of Lower Triassic in the footwall;. Locations of A-E are shown in Fig. 7. Location of F is shown in Fig. 9.

Fig. 6. Stratigraphic columns and framework of the Cretaceous in the Jianghan Basin. Data for stratigraphic columns of the northwest and northeast basins are from (CM, 1970; YM, 1970, 1976; HBGMR, 1990) as well as our field investigation. Two selected wells, Eshen13 and Hai9, show the generalized stratigraphy of the Upper Cretaceous strata in most of the Jianghan Basin. Stratigraphic units: E = Paleogene, T_2 = Middle Triassic, O = Ordovician, Є = Cambrian. Well locations are shown in Fig. 4.

Fig. 7. (A-C) Maps showing the distribution of the Lower Cretaceous strata in the Jianghan Basin (modified from CM, 1970; YM, 1970, 1976). D, cross section showing the stratal relationships of the Cretaceous (modified from YM, 1970).

Fig. 8. (A) Structural Map of the Jianghan Basin, illustrating the distribution of major faults and Late Cretaceous units. The inserted rose diagrams show the strikes of the Late Cretaceous faults. The strike data are length-weighted. The faults initiated during the Late Cretaceous are marked by solid lines while faults initiated during the Paleogene are marked by dashed lines. (B) Vertical thickness map of the Upper Cretaceous strata. Residual thickness is used to approximately reflect the original thickness, due to limited erosion. The contour interval is 600 m. Fault data and stratal thickness beyond the seismic and drilling well coverage is from (NM, 1965; YM, 1965; CM, 1970;

YM, 1970, 1976; HBGMR, 1990). Fault names: WF = Wancheng Fault, ZFZ = Zibei Fault Zone, PF = Pujiguan Fault, QF = Qianbei Fault, ZF = Zhugentan Fault, TF = Tonghaikou Fault, NF = Nanmiao Fault, HF = Honghu Fault, DF = Datonghu Fault, CF = Chahekou Fault.

Fig. 9. Structural cross sections of the north Jianghan Basin. Section A-A', modified after Shi et al. (2013); Section B-B', modified from ZM (1976). Stratigraphic units: N+Q = Neogene-Quaternary, E = Paleogene, K_2 = Late Cretaceous, T_2-J = Middle Triassic to Jurassic, D-T_1 = Devonian-Lower Triassic, S = Silurian, Є-O = Cambrian-Ordovician, Z = Sinian, Pt = Proterozoic. Stratigraphic units are consistent and referred to throughout the text. Neogene-Quaternary strata in the Hanshui graben are not shown, due to their limited thicknesses. See Figs. 4 and 8A for location.

Fig. 10. Interpreted seismic sections across the Hanshui Fault (A, B), Wen'ansi Fault and Wancheng Faults (C). Stratigraphic units are as in Fig. 9. Well located nearby the profile is indicated by vertical dashed line. See Figs. 4 and 8A for location. Uninterpreted seismic sections are provides as online supporting files (Fig. A2).

Fig. 11. Interpreted seismic sections across the Zibei Fault Zone (A), Tianmenhe Fault (B) and Datonghu Fault (C). CF = Chahekou Fault. The faults initiated during the Paleogene are marked by pink in Fig. 11A. Stratigraphic units are as in Fig. 9. See Figs. 4 and 8A for location. Uninterpreted seismic sections are provides as online supporting files (Fig. A3).

Fig. 12. (A) The distribution of Cretaceous magmatic rocks and rift basins in the South China Block

(modified after Li et al., 2014b). (B) The distribution of the Triassic to Jurassic magmatic rocks in the South China Block (modified after Zhou et al., 2006; Li et al., 2012c). See Fig. 1A for location.

Fig. 13. Map showing the deformation of pre-rift basement during the Late Jurassic. The location and orientation of thrust faults were inferred from the major rift-related faults shown in Fig. 8. Data in the outcrop area are from HBGMR (1988, 1990) and relevant stratigraphic information is shown in Fig. 2. Thrust directions are shown schematically, which are inferred based on the fold traces and discussion in published literatures (Shi et al., 2013; Liu et al., 2015). The thrust directions of the Southern Qinling-Dabie Thrust Belt and Northern Jiangnan Thrust Belt are marked by blue and violet arrows, respectively. The obstruction of the Huangling Massif is shown with pale blue columns. The “obstruction” means that the Huangling Massif was a relatively rigid and passive block, being squeezed by the Qinling-Dabie Orogenic Belt and Jiangnan Orogen.

Fig. 14. Cartoon diagrams illustrating the initial rifting processes and geodynamics of the Jianghan Basin. The lithospheric thinning processes are modified on the basis of flat-slab subduction model of the South China Block (Li and Li, 2007) and thinning/destruction model of the eastern North China Block (Li et al., 2012a; Zhu et al., 2015). Basalt eruptions are presented schematically based on the drilling data shown in Fig. 4. The indigo line shows the location of cross section in the front. The horizontal extension amounts of the lithosphere are not displayed.

Table caption

Table 1 Biostratigraphic correlation of the Cretaceous Jianghan Basin (Lei et al., 1987; HBGMR, 1990). The maximum depositional ages are from Shen et al. (2012a). The depositional ages of each unit are shown in parentheses.

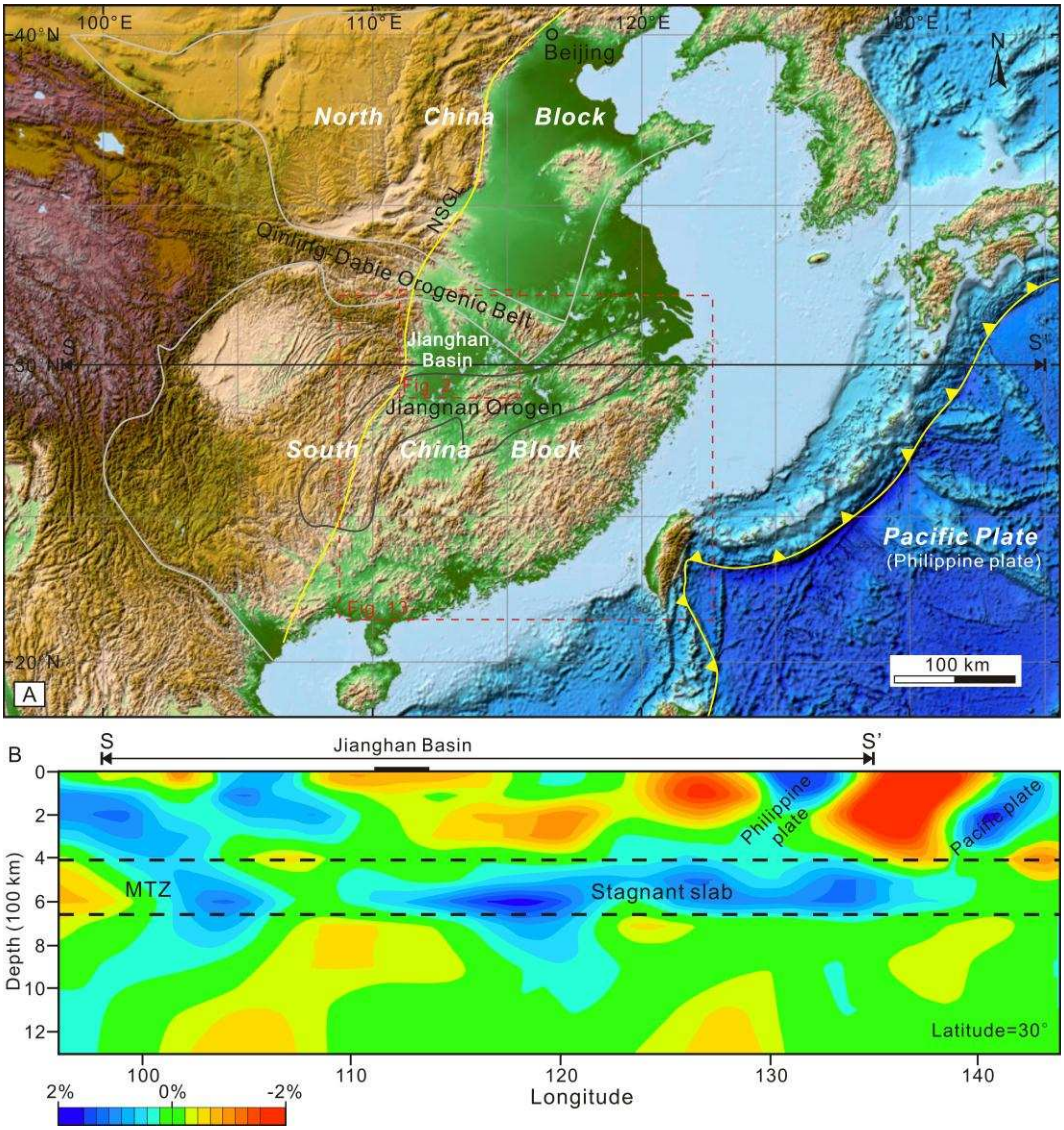

Fig. 1 (A) Simplified map showing the topography and tectonic divisions of southern Eastern Asia. (B) Vertical section of P wave velocity perturbations across the western Pacific-eastern China at the latitude 30ºN (after Huang and Zhao, 2006), showing the Pacific slab lying horizontally in the mantle transition zone (MTZ). Topography map is based on Etopo 1 (Amante and Eakins, 2009). Tectonic divisions are modified from Li and Li (2007), Mei et al. (2012), Zhu et al. (2015). NSGL, North-South Gravity Lineament (modified from Ma, 1989).

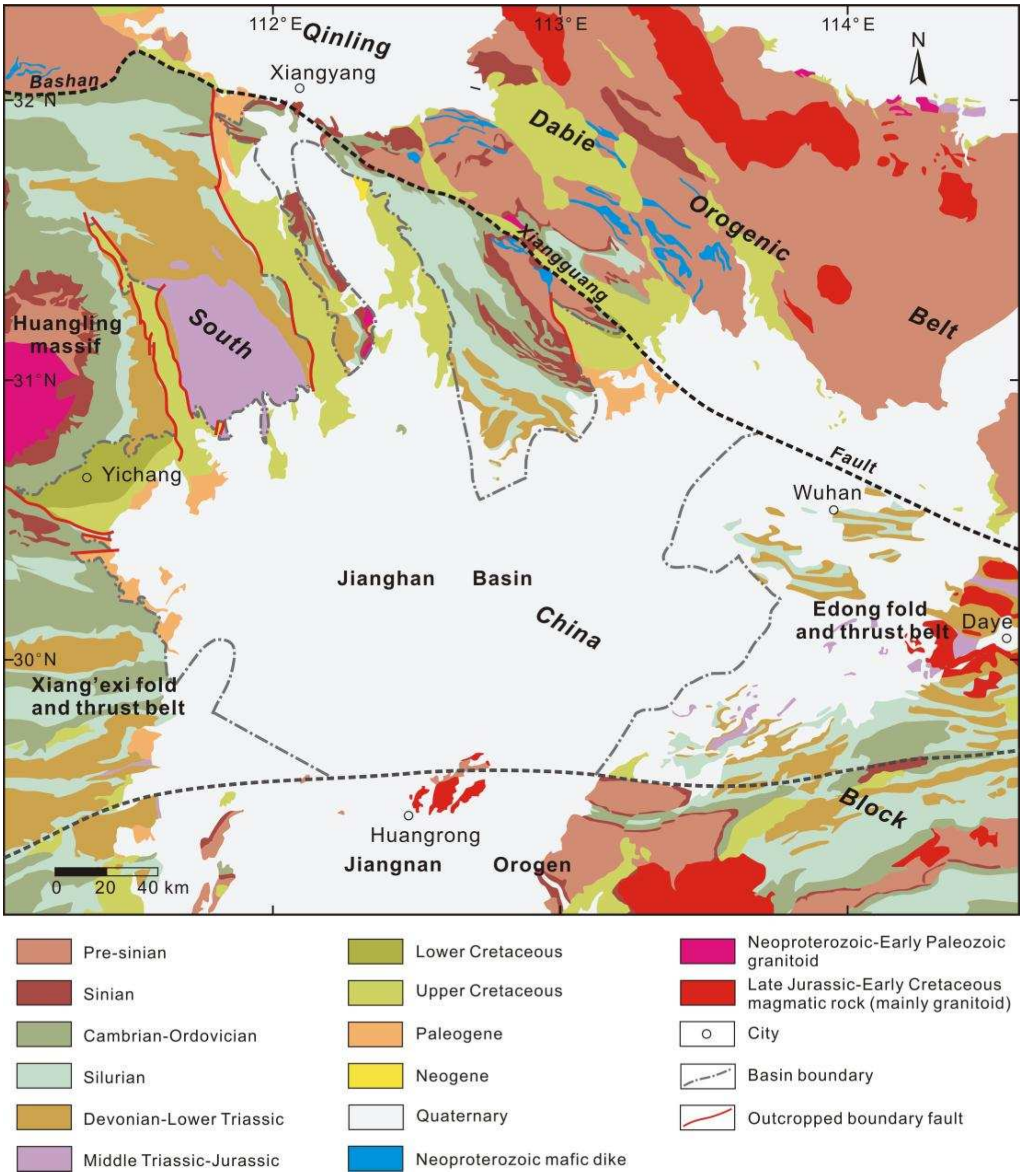

Fig. 2 Geological map of the Jianghan basin and adjacent areas, modified after HBGMR, 1988, 1989, 1990. See Fig. 1 for location.

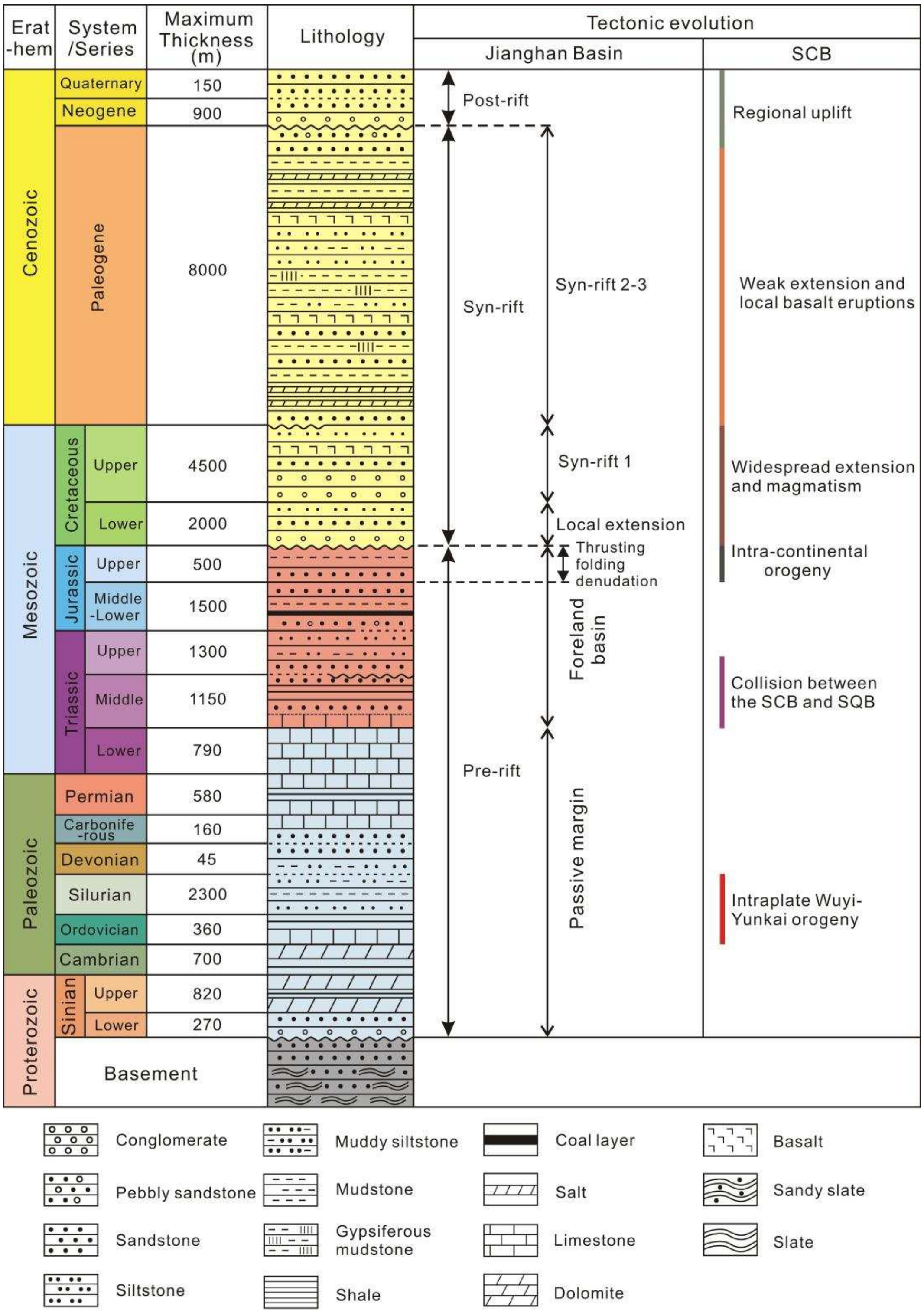

Fig. 3 Tectonostratigraphic chart for the Jianghan Basin showing the lithostratigraphic characteristics, basin evolution and main regional events (modified from HBGMR, 1988, 1989, 1990; Dong et al., 2011; Wang et al., 2013b; Li et al., 2014b; Yao et al., 2015). SCB, South China Block; SQB, South Qinling Belt.

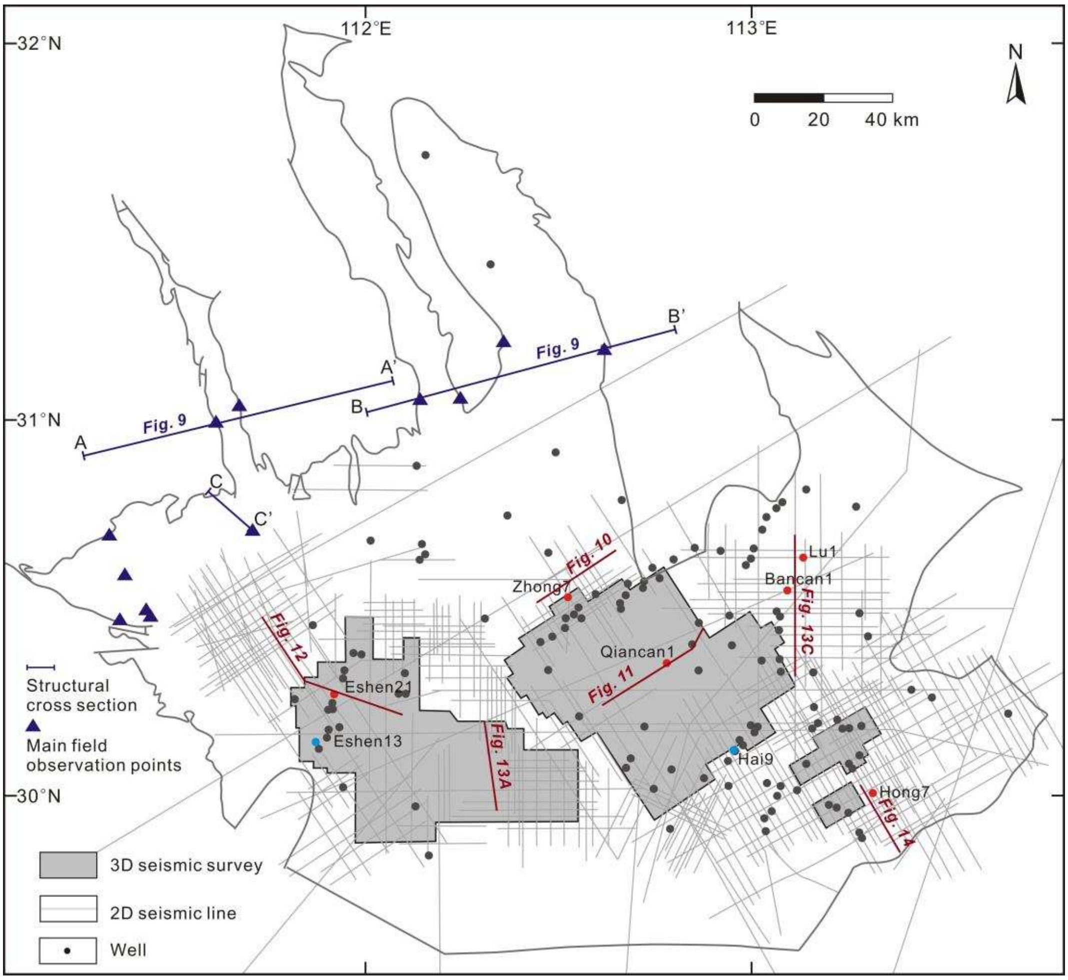

Fig. 4 Map showing the coverage of 2-D and 3-D seismic reflection data and drilling wells penetrating the Upper Cretaceous and /or pre-rift basement, along with two structural cross sections and main field observation points. Wells marked by blue and red dots are shown in Figs. 6 and 10-14, respectively.

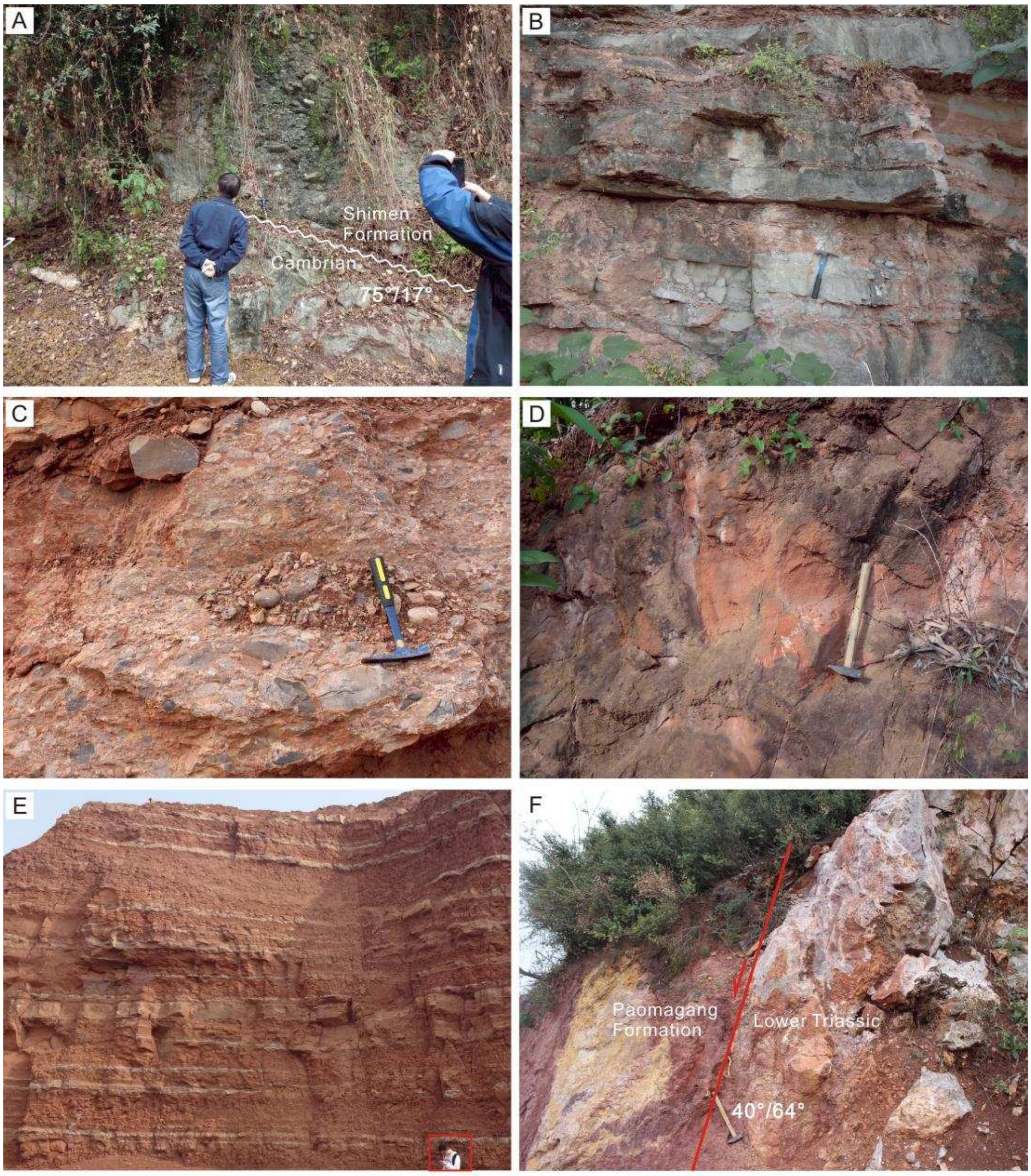

G

System	Series	Formation					Sedimentary cycle
		Northwest Basin	Fig.	Northeast Basin	Central and south Basin	Fig.	
Cretaceous	Upper	Paomagang	5E	Yuntaishan	Yuyang	6	Fining -upward
		Honghuatao	5D	Gong'anzhai			
		Luojingtan	5C	Hejiapo			
	Lower	Wulong	5B	Quanshuihe			Fining -upward
		Shimen	5A				

Fig. 5 lithostratigraphic feature of the Cretaceous in the Jianghan Basin. A, Shimen Formation, gray conglomerate transgressed on the Cambrian dolomite above an unconformity; B, Wulong Formation, gray sandstone with interbedded brick-red mudstone; C, Luojingtan Formation, gray-red conglomerate; D, Honghuatao Formation, brick-red sandstone; E, Paomagang Formation, brown-red mudstone with interbedded gray-green siltstone and sandstone; F, Jingmen Fault, purple-red sandstone of Paomagang Formation in the hangingwall and gray-white limestone of Lower Triassic; G, stratigraphic framework and correlation (HBGMR, 1990; Xu et al., 1995; Wang et al., 2014). Locations of A-E are shown in Fig. 7. Location of F is shown in Fig. 9.

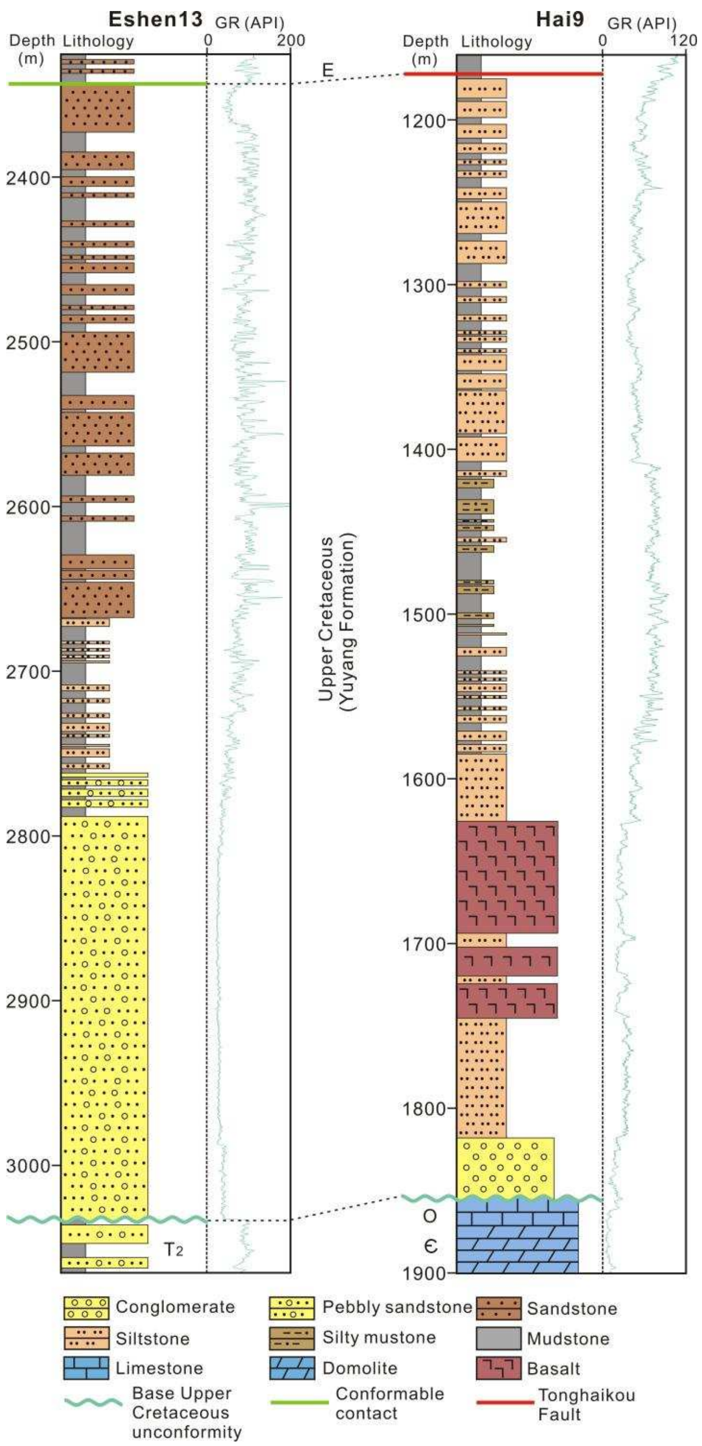

Fig. 6 lithostratigraphic clolumns of two selected wells showing the stratigraphy of the Upper Cretaceous in the inner Jianghan Basin, along with gamma ray logs. Stratum symbols: E = Paleogene, T_2 = Middle Triassic, O = Ordovician, Є = Cambrian. Well locations are shown in Fig. 4.

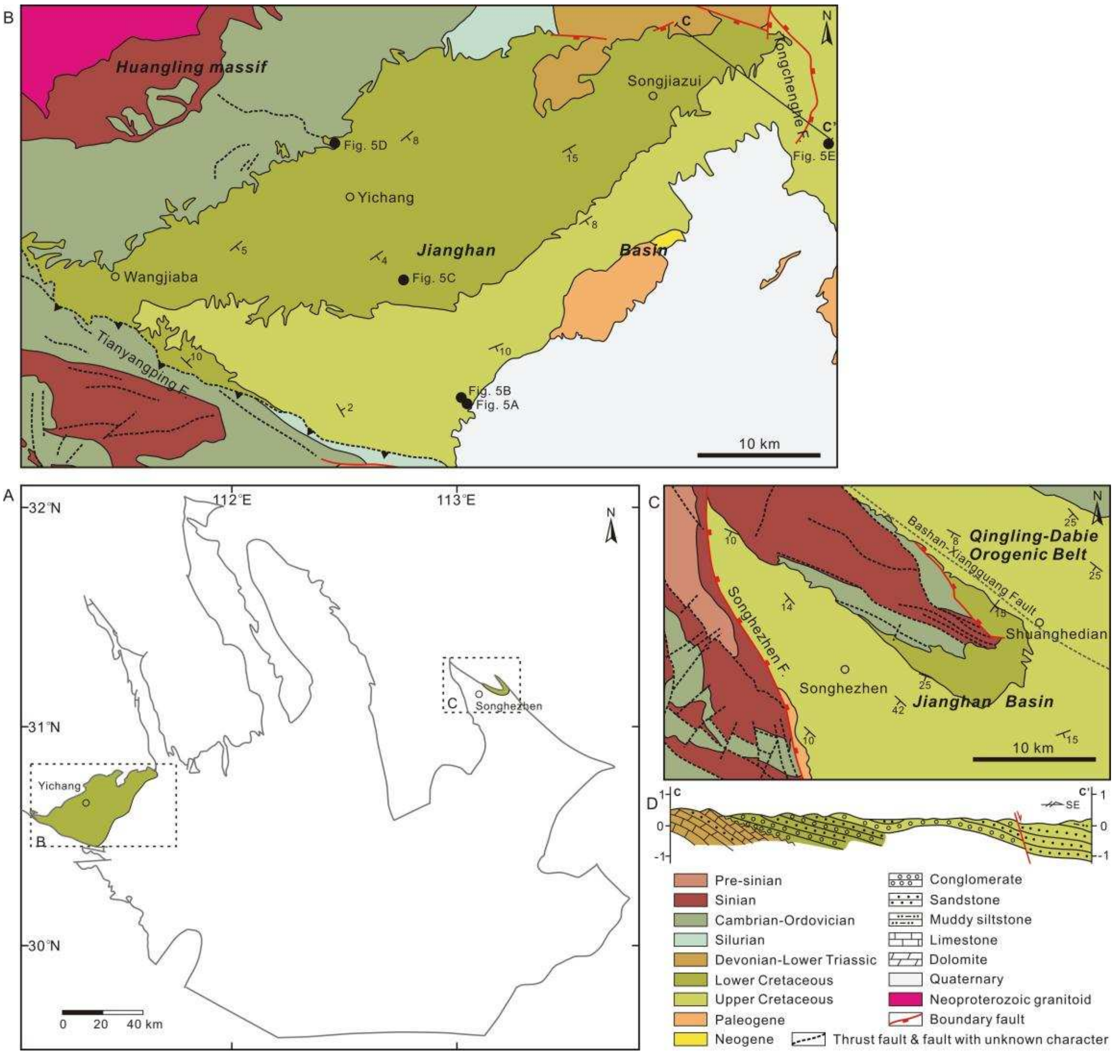

Fig. 7 (A-C) Maps showing the distribution of the Lower Cretaceous in the Jianghan Basin (modified from CM, 1970; YM, 1970, 1976). D, cross section showing the filled characteristics of the Lower Cretaceous (modified from YM, 1970).

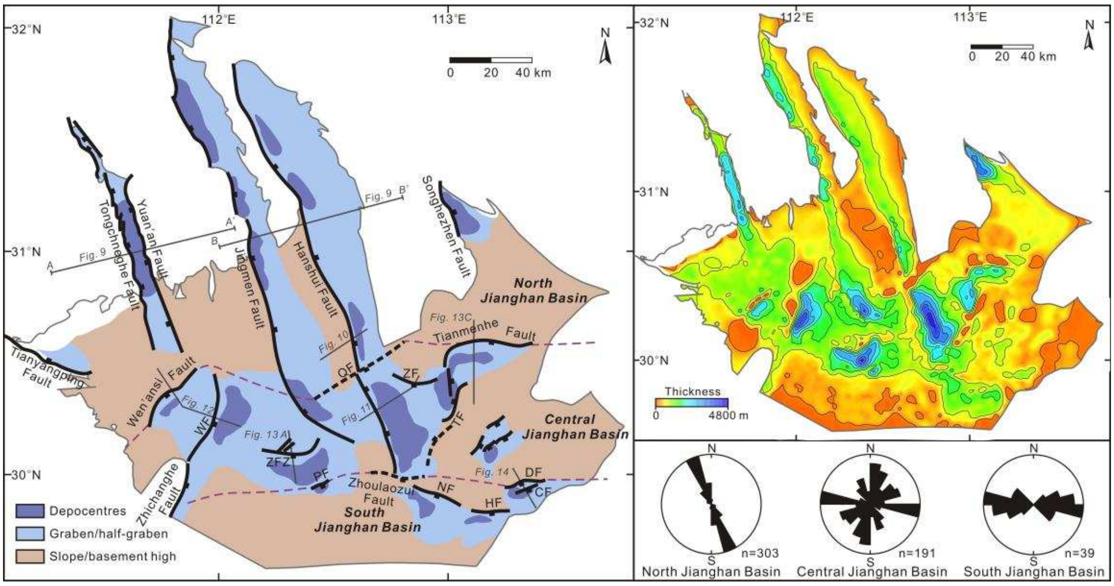

Fig. 8 (A) Structural Map of the Late Cretaceous Jianghan Basin, illustrating the distribution of major faults and related units. Data of faults and stratal thickness beyond the seismic and drilling well coverage is from (NM, 1965; YM, 1965; CM, 1970; YM, 1970, 1976; HBGMR, 1990). The faults initiated during the Late Cretaceous are marked by solid lines while faults initiated during the Paleogene are marked by dashed lines. (B) Vertical thickness map of the Upper Cretaceous. Residual thickness is used to approximately reflect the original thickness as the denudation is limited on the whole. (C) Rose diagrams showing the strikes of the Late Cretaceous faults. The strike data are length-weighted. Fault names: WF = Wancheng Fault, ZFZ = Zibei Fault Zone, PF = Pujiguan Fault, QF = Qianbei Fault, ZF = Zhugentan Fault, TF = Tonghaikou Fault, NF = Nanmiao Fault, HF = Honghu Fault, DF = Datonghu Fault, CF = Chahekou Fault.

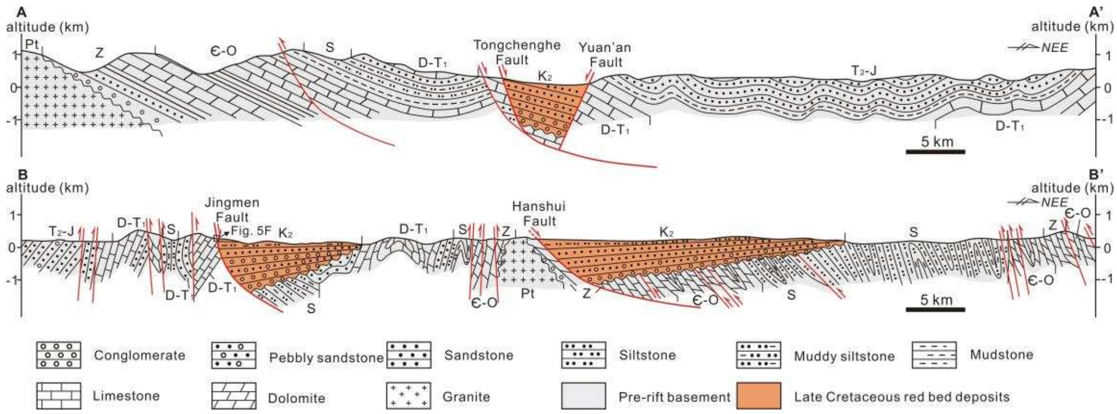

Fig. 9 Structural cross sections of the north Jianghan Basin. Section A-A', modified after Shi et al. (2013); Section B-B', modified from ZM (1976). Stratum symbols: N+Q = Neogene-Quaternary, E = Paleogene, K_2 = Lower Cretaceous, T_2-J = Middle Triassic to Jurassic, D-T_1 = Devonian-Lower Triassic, S = Silurian, Є-O = Cambrian-Ordovician, Z = Sinian, Pt = Proterozoic. Stratum symbols are consistent and referred to throughout the text. Neogene-Quaternary in the Hanshui graben are ignored for their limited thicknesses. See Figs. 4 and 8A for location.

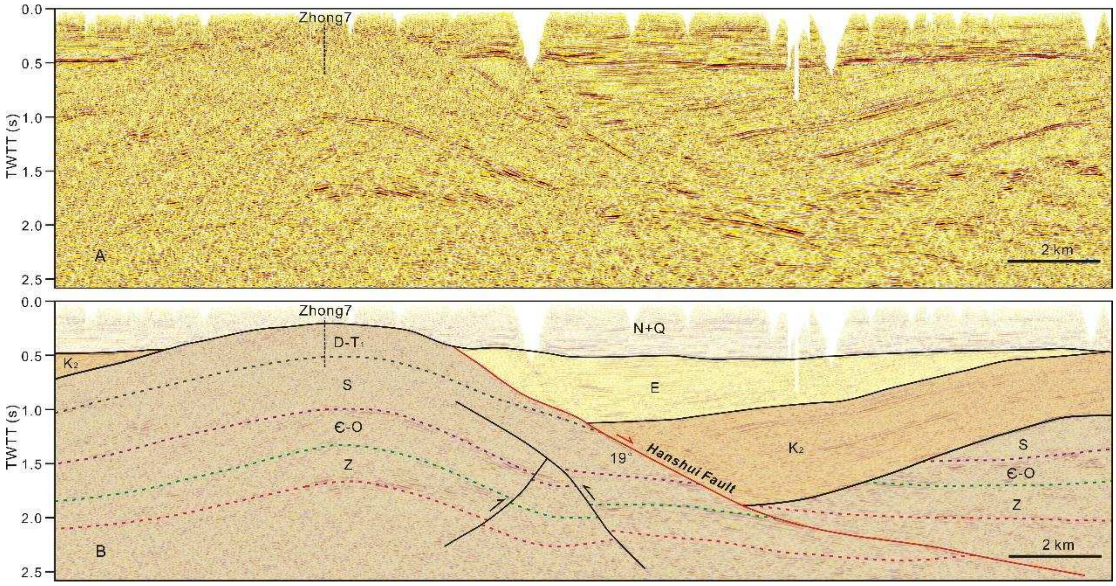

Fig. 10 Uninterpreted and interpreted seismic sections across the Hanshui Fault in the north Jianghan Basin. Stratum symbols are as in Fig. 9. Zhong7 well located nearby the profile is indicated by vertical dashed line. See Figs. 4 and 8A for location.

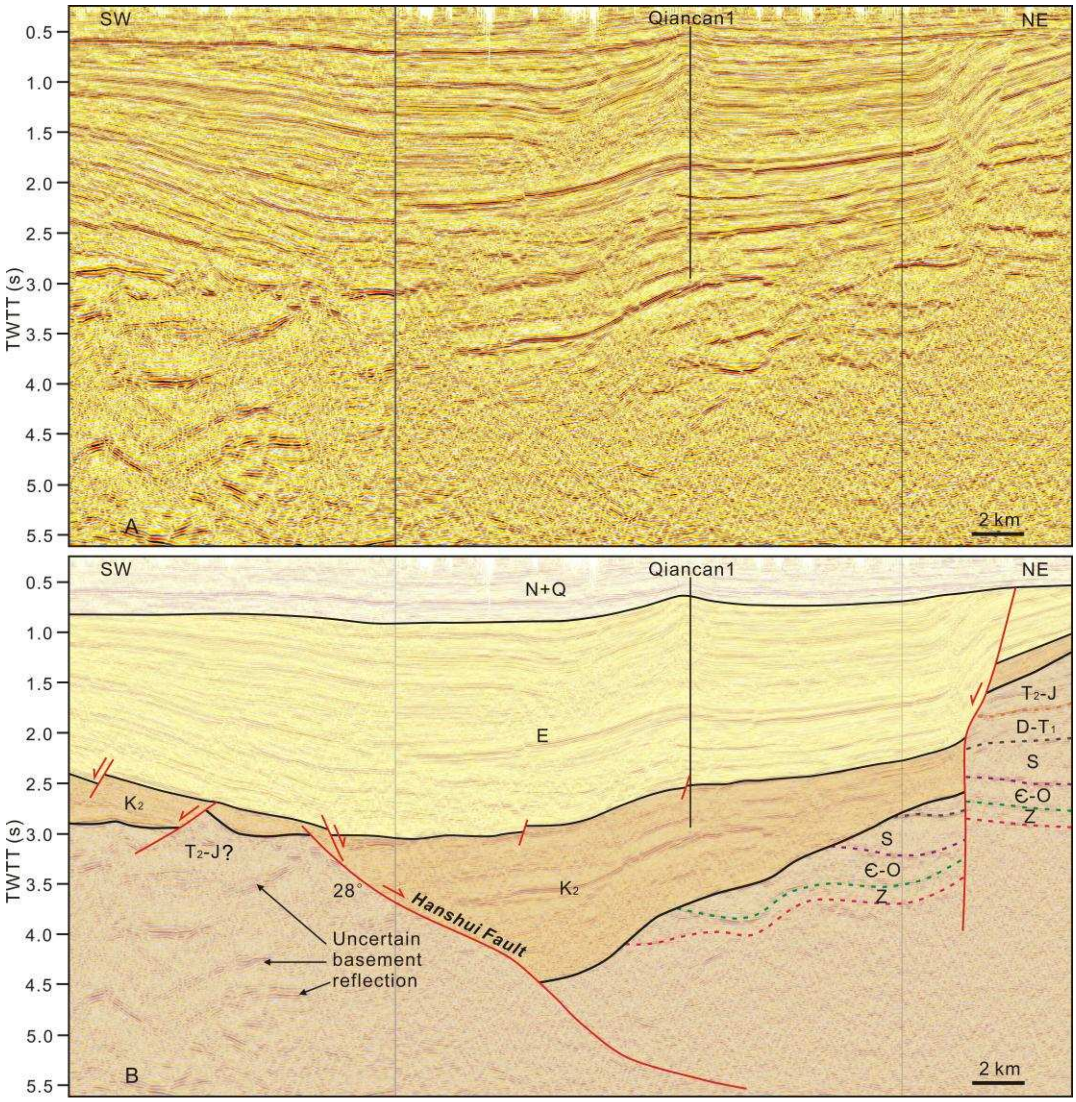

Fig. 11 Uninterpreted and interpreted seismic sections across the southern segment of Hanshui Fault in the central Jianghan Basin. Stratum symbols are as in Fig. 10. See Figs. 4 and 8A for location.

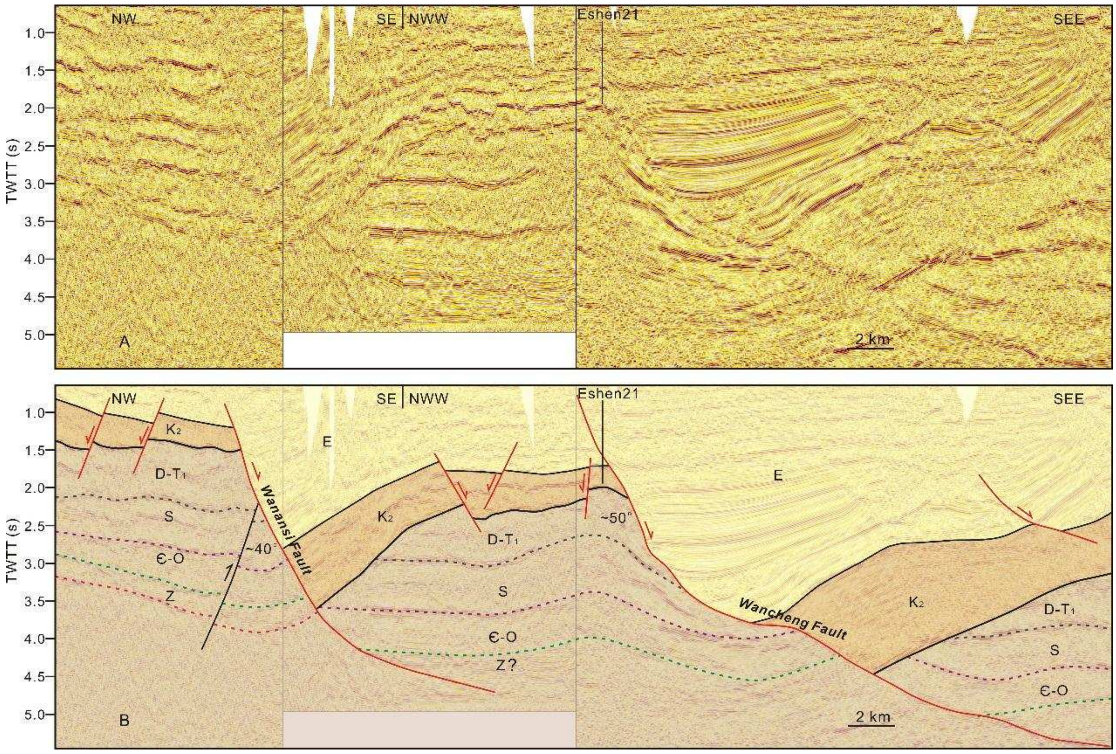

Fig. 12 Uninterpreted and interpreted seismic sections across the Wen'ansi and Wancheng Faults in the central Jianghan Basin. Stratum symbols are as in Fig. 9. See Figs. 4 and 8A for location.

Fig. 13 Uninterpreted and interpreted seismic sections across the Zibei Fault Zone (A, B) and Tianmenhe Fault (C, D). The faults initiated during the Paleogene are marked by pink in Fig. 11B. Stratum symbols are as in Fig. 9. Bancan1 well located nearby Line 5 is indicated by vertical dashed line. See Figs. 4 and 8A for location.

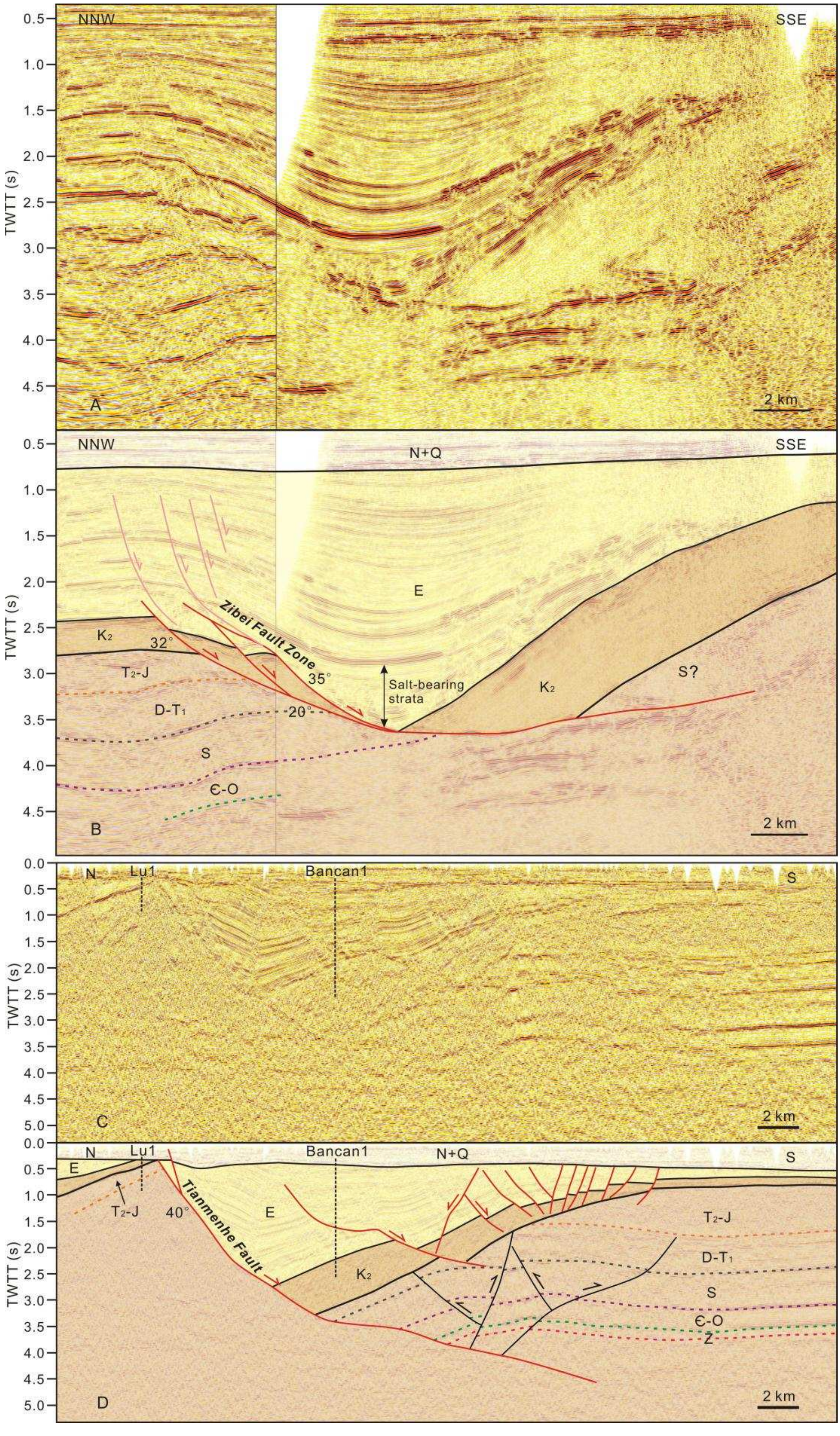

NNW
SSE
TWTT (s)
A
2 km
NNW
N+Q
SSE
E
K2
32°
Zibei Fault Zone
35°
T2-J
Salt-bearing strata
K2
S?
D-T1
20°
S
Є-O
B
2 km
N
Lu1
Bancan1
S
TWTT (s)
C
2 km
N
Lu1
Bancan1
N+Q
S
E
T2-J
40°
E
Tianmenhe Fault
K2
T2-J
D-T1
S
Є-O
Z
D
2 km

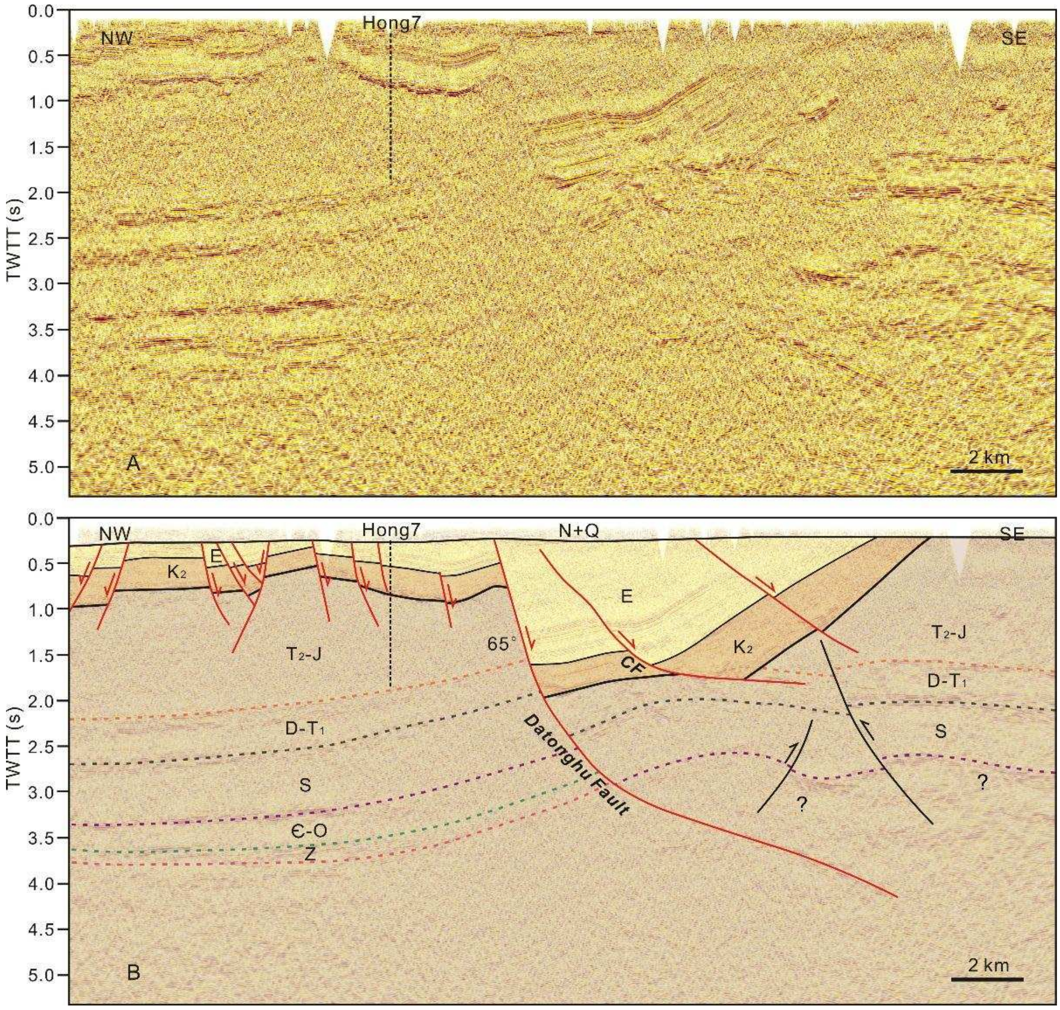

Fig. 14 Uninterpreted and interpreted seismic sections across the Datonghu Fault in the south Jianghan Basin. CF = Chahekou Fault. Stratum symbols are as in Fig. 9. Hong7 well located nearby the profile is indicated by vertical dashed line. See Figs. 4 and 8A for location.

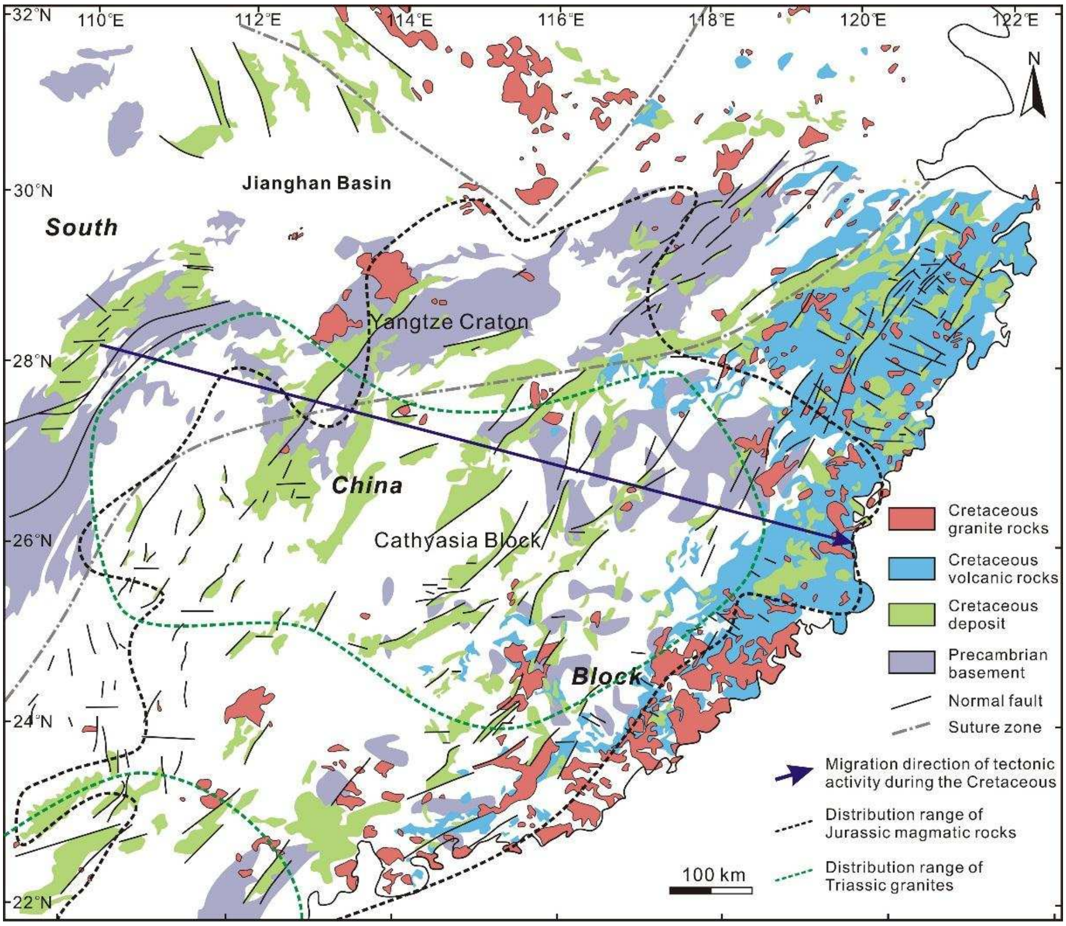

Fig. 15 Simplified geological map of the South China Block showing the distributions of Cretaceous structures and magmatic rocks (modified after Li et al., 2014b), along with the distributions of the Triassic to Jurassic magmatic rocks (modified after Zhou et al., 2006; Li et al., 2012c). See Fig. 1 for location.

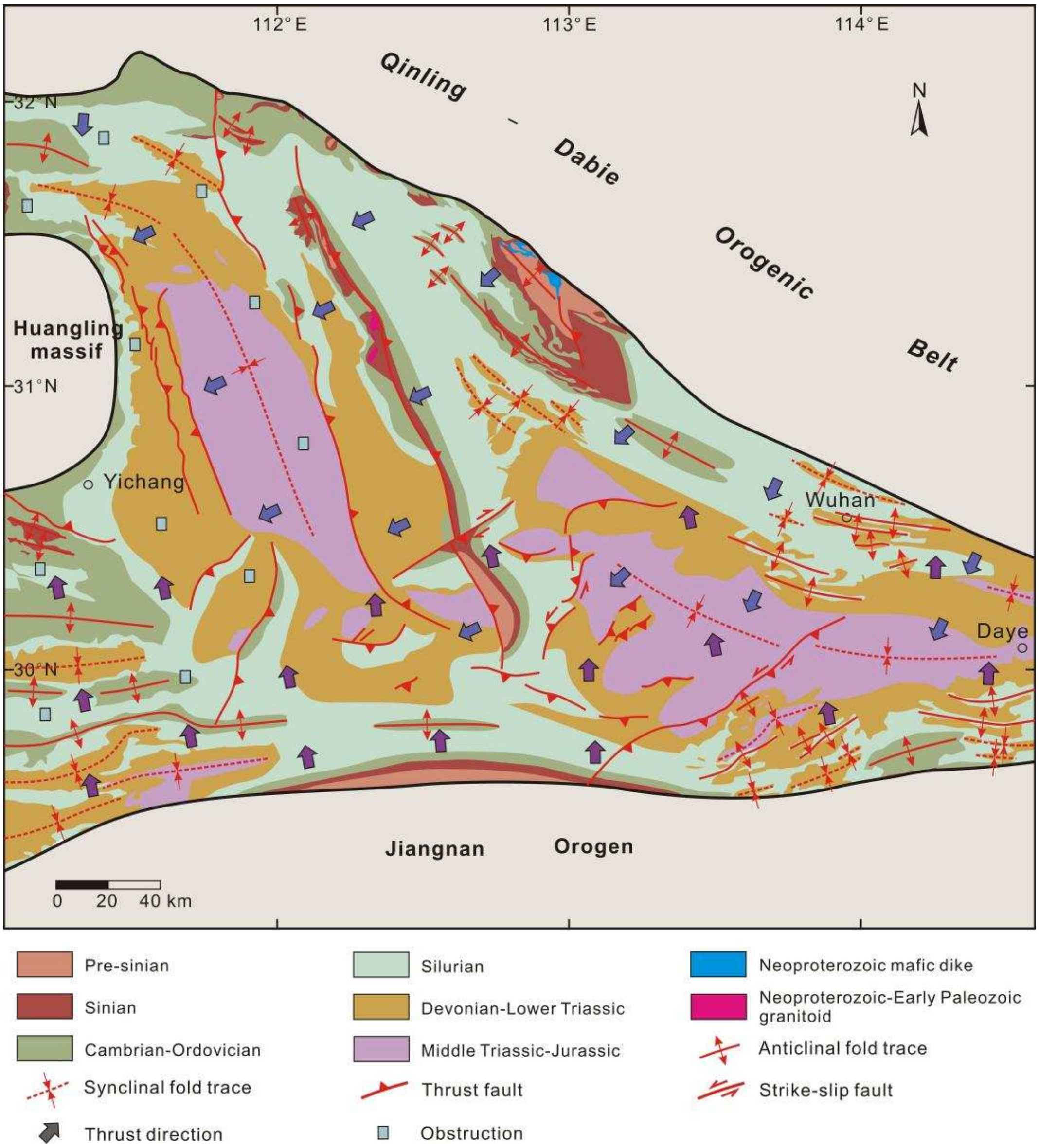

Fig. 16 Map showing the deformation characteristics of pre-rift basement during the Late Jurassic. The location and orientation of thrust faults were inferred from the major rift-related faults shown in Fig. 8. Data in the outcrop area is from HBGMR (1988, 1990) and relevant stratigraphic information is shown in Fig. 2. Thrust directions are shown schematically, which are inferred based on the fold traces and discussion in published literatures (Shi et al., 2013; Liu et al., 2015). The thrust directions of the Southern Qinling-Dabie Thrust Belt and Northern Jiangnan Thrust Belt are marked by blue and violet arrows, respectively. The obstruction of the Huangling massif is shown with pale blue columns.

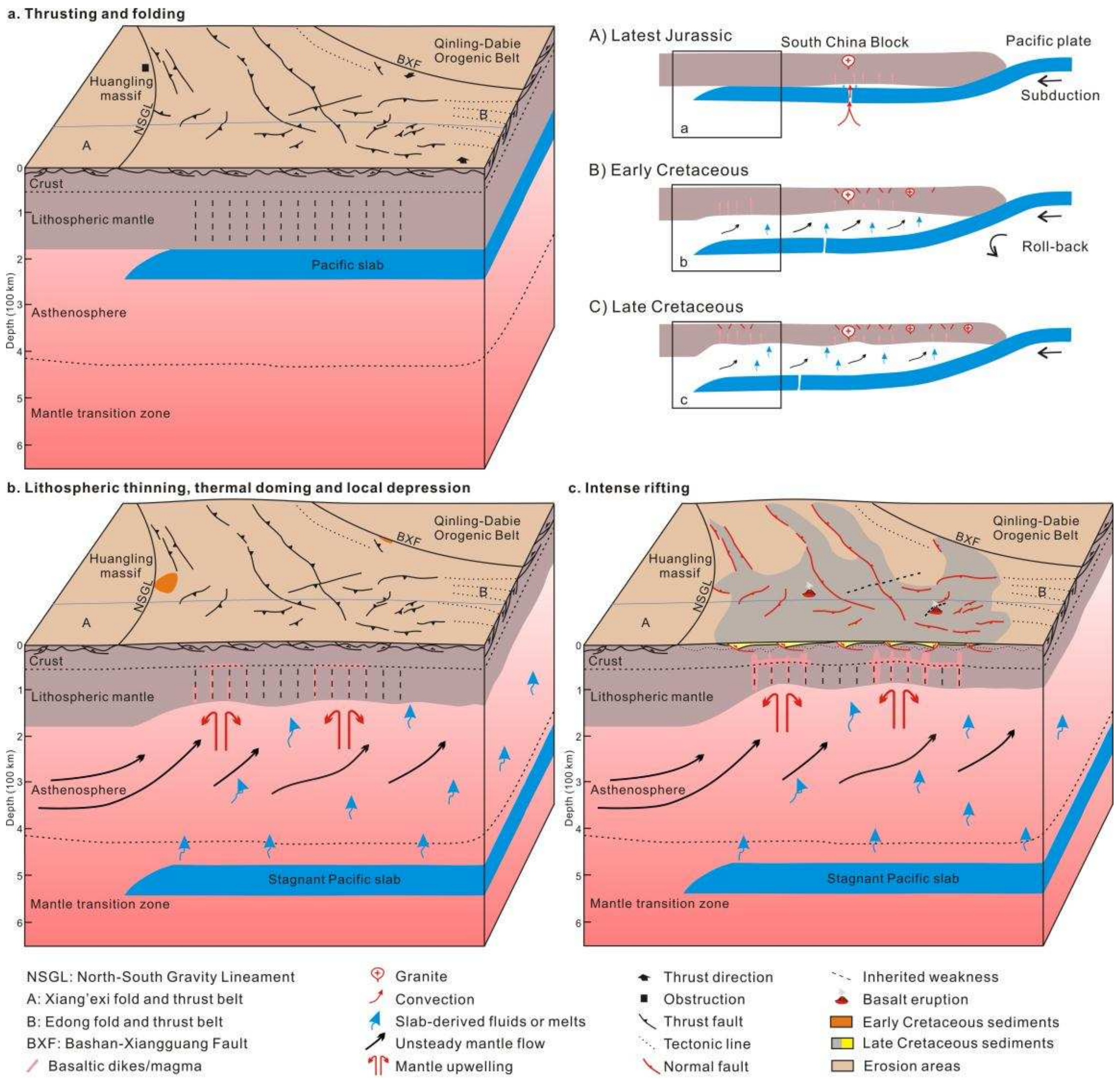

Fig. 17 Cartoon diagrams illustrating the initial rifting processes and geodynamics of the Jianghan Basin. The lithospheric thinning processes are modified on the basis of flat-slab subduction model of the South China Block (Li and Li, 2007) and thinning/destruction model of the eastern North China Block (Li et al., 2012a; Zhu et al., 2015). Basalt eruptions are shown schematically based on the drilling data shown in Fig. 4. The indigo line shows the location of cross section in the front.